*J. Fluid Mech.* (1994), *vol.* 261, *pp.* 223–252



# The evolution of capillary fountains

By R. M. S. M. SCHULKES†

Department of Applied Mathematics and Theoretical Physics, University of Cambridge, Silver Street, Cambridge CB3 9EW, UK

(Received 22 March 1993 and in revised form 30 August 1993)

In this paper we consider the dynamics of a growing capillary fountain. We assume that at some time $t = 0$ an inviscid incompressible fluid is ejected vertically upwards through a circular nozzle. The subsequent dynamics of the resulting fountain is studied numerically using the boundary-element technique. The rate at which fluid is discharged from the nozzle and the Bond number (a measure of gravitational and surface tension forces) are the parameters that govern the dynamics of the fountain. For small discharge rates the fountain assumes the form of a slowly growing sessile drop, with dynamic effects not modifying the shape of the drop significantly. For large discharge rates we find that close to the symmetry axis a region develops with a high curvature. This strongly curved region results in a physical instability which can take on one of two forms: either a liquid drop is ejected from the free surface or the capillary surface entrains a bubble. For intermediate values of the discharge rate we find that fluid lobes develop which fall over the side of the nozzle. A number of experimental results are also presented showing the evolution of water fountains for different Bond numbers and discharge rates. Some of our numerical predictions are confirmed by the experimental results.

## 1. Introduction

Fountains, widely varying in size and design, are often used for decoration in gardens and buildings. The structure of these fountains is usually highly irregular and time dependent: the maximum height varies significantly with time and the break-up of the fountain into a spray of drops can often be observed. While in many cases the irregular behaviour of the fountain is enhanced by external effects (such as wind and irregularities in the nozzle and exit velocity), even seemingly well-constructed fountains in a shielded environment exhibit this irregular behaviour. It appears that there is no stable configuration for the fountain, thus preventing a steady state to be reached.

For small exit velocities of the fluid, a stable configuration of the fountain may exist. The fountain would presumably evolve to a well-like structure with fluid overflowing the nozzle in a symmetric way. This particular problem has been studied by Dias & Vanden-Broeck (1990). Under the assumptions that the fluid attaches to the outside of the nozzle and that cavitation does not occur near the mouth of the nozzle, Dias & Vanden-Broeck have calculated the (two-dimensional) flow emerging from an infinitely long rectangular slit. Under the assumption that a stable, steady state exists, Vanden-Broeck (1993) recently calculated the asymptotic shape of a two-dimensional jet aimed vertically upwards. While the work of Dias & Vanden-Broeck (1990) and Vanden-Broeck (1993) gives important insight into the shape of the free surface, interesting questions related to the initial evolution of the fountain as it emerges from the nozzle

† Present address: School of Mathematics, University of East Anglia, Norwich NR4 7TJ, UK.

have not been answered. Another important question related to the aforementioned articles is whether it is at all possible to obtain a stable steady flow emerging from a nozzle pointed vertically upwards.

It is clear that the exit velocity of the fluid emerging from the nozzle is an important parameter on which the stability of the resulting fountain may depend: high exit velocities appear to yield an unstable configuration while for small exit velocities a stable configuration may exist. Questions related to the stability of a fountain can only be answered by studying the evolution of the fountain as it emerges from the nozzle. Notwithstanding the highly irregular behaviour of a fully developed fountain which results when fluid is ejected at a large speed, the structure of the fountain as it first emerges from the nozzle is likely to be symmetric when the nozzle is symmetric. Instabilities may develop for large ejection velocities which, in practice, would lead to the observed irregular behaviour. By studying the evolution of the fountain we can also investigate whether cavitation occurs at the mouth of the nozzle.

Questions related to the initial development of the flow that is ejected from a nozzle have, to our knowledge, not been investigated previously. An important physical effect which has to be incorporated whenever the initial development of the fountain is studied, is surface tension. Without surface tension, the fluid region leaving the nozzle would initially have sharp edges, which is clearly non-physical. Surface tension effects are very important for nozzles with a small radius. However, even for nozzles with a relatively large radius we find that surface tension effects lead to rather surprising physical phenomena. For example, numerical and physical experiments show that a drop may be ejected from the capillary surface when, for a given nozzle size, the discharge rate is above a certain critical value. The ejection of the drop is due to the formation of a concave region with a large curvature near the symmetry axis of the fountain. The formation of the concave region is entirely due to the presence of surface tension forces.

The problem of the fluid emerging from a nozzle is clearly a free-boundary problem: the area of the capillary free surface increases rapidly in time, with the shape of the free boundary undergoing extremely large deformations. In order to study this problem, great gains can be made by taking the fluid to be inviscid and incompressible and assuming the flow to be irrotational. The resulting problem, in which the fluid velocity can be expressed in terms of a velocity potential, presents a natural basis for an integral formulation which is of particular interest when one is primarily concerned with the dynamics of a free boundary. A large body of literature exists in which an integral formulation has been applied to a variety of potential flows involving free boundaries. If we restrict ourselves to the literature involving the dynamics of (axisymmetric) capillary surfaces we find only a small number of papers. Nonlinear oscillations of liquid drops were studied by Lundgren & Mansour (1988) and Pelekasis, Tsamopoulos & Manolis (1992) while the dynamics of liquid shells was the subject of a study by Pelekasis, Tsamopoulos & Manolis (1991). The impact of a drop on a liquid surface has been investigated in a number of articles, see for example Oğuz & Prosperetti (1990*a*).

A common denominator in almost all numerical studies employing an integral formulation of potential-free-surface flows is the appearance of short-wavelength instabilities. While various techniques haven been used to eliminate these instabilities, the underlying mechanism causing the instabilities is still a subject of some discussion. It is not our aim in this paper to enter into a detailed discussion of the short-wavelength instabilities, for this the reader is referred to Dold (1992) and Pelekasis *et al.* (1992). In the work presented here, short-wavelength instabilities were also found to be present.

However, at least as important as the prevention of these instabilities is the control of the numerical discretization error. In the problems we have considered, the volume of fluid bounded by the capillary surface increases linearly with time. Owing to the incompressibility of the fluid, it follows that the surface area of the capillary surface must increase proportional to $t^{\frac{2}{3}}$. This implies that the number of nodes on the capillary surface must increase continuously in order to control the discretization error. A mechanism to add nodes to the free surface in a well-defined manner to control the discretization error and to prevent the occurrence of short-wavelength instabilities is a crucial aspect of the numerical implementation presented here to study the evolution of capillary fountains.

In §2 we present the governing equations which are written in integral form. Details of the numerical discretization are discussed in §3. Owing to the enormous movement of Lagrangian nodes, extensive regridding is required in order to prevent certain regions of the fountain being completely devoid of nodes. This is in addition to the fact that short-wavelength instabilities are observed whenever two Langrangian nodes move too close together. No explicit smoothing is used since the regridding operation was sufficient to prevent the occurrence of instabilities. Our regridding strategy and the choice of the time-integration scheme are discussed in §4 and results of our calculations are presented in §5. In §6 we present some experimental results which appear to confirm some of our numerical predictions. Finally, in §7 we present our conclusions.

## 2. Problem formulation

The problem to be considered in this paper is shown schematically in figure 1. A cylindrical nozzle with radius $R$ is positioned such that the outlet points vertically upwards. We assume that initially the capillary surface is flat and situated at the mouth of the nozzle. At some time $t = 0$ fluid is ejected from the nozzle at a constant rate resulting in a capillary fountain above the nozzle. Let the (time-dependent) domain occupied by the fluid be denoted by $\Omega(t)$. The boundary of $\Omega(t)$, denoted by $\partial\Omega$, consists of three different parts: a capillary free boundary denoted by $S(t)$, the rigid side of the nozzle denoted by $B$ and a boundary $\Gamma$ on which the normal velocity is prescribed. We assume that $\Omega(t)$ is axisymmetric, and henceforth $\partial\Omega$, $S(t)$, $B$ and $\Gamma$ denote curves in the $(r, z)$-plane. The $z$-axis, pointing vertically upwards, is taken to be the symmetry axis of our domain and the gravitational force acts downwards along the negative $z$-axis.

The governing equations will be written in dimensionless form with the radius of the nozzle as the characteristic lengthscale; the characteristic timescale is given by $T = (\rho R^3/\sigma)^{\frac{1}{2}}$ ($\rho$ is the fluid density and $\sigma$ is the coefficient of surface tension) and a pressure scale is given by $P = \sigma/R$. We assume that $\Omega(t)$ is occupied by an inviscid incompressible fluid. The flow is assumed to be irrotational and hence the velocity field in $\Omega(t)$ can be described by a velocity potential $\phi$ which satisfies Laplace's equation. Rotational symmetry in a cylindrical coordinate system yields

$$\frac{\partial^2\phi}{\partial r^2} + \frac{1}{r}\frac{\partial\phi}{\partial r} + \frac{\partial^2\phi}{\partial z^2} = 0. \tag{1}$$

The rigid side $B$ of the nozzle is situated at $r = 1$ while we assume that the nozzle inlet $\Gamma$ is positioned at $z = 0$ and the nozzle outlet is at $z = 1$. The boundary condition on $B$ is given by

$$\left.\frac{\partial\phi}{\partial r}\right|_{r=1} = 0, \tag{2}$$

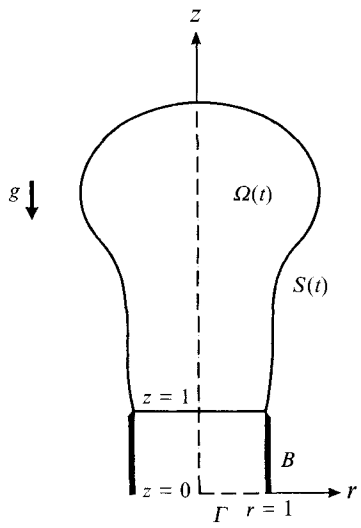


FIGURE 1. Schematic diagram of a capillary fountain.

while the normal velocity is prescribed on $\Gamma$, giving

$$\left.\frac{\partial\phi}{\partial z}\right|_{z=0} = We^{\frac{1}{2}}\Psi(r), \tag{3}$$

in which $\Psi(r)$ denotes the dimensionless flux and $We = \rho RV^2/\sigma$ is the Weber number with $V$ a measure of the normal velocity.

Three boundary conditions are specified on the capillary free surface $S(t)$: two kinematic conditions, namely

$$\frac{Dr}{Dt} = \frac{\partial\phi}{\partial r} = n_r\frac{\partial\phi}{\partial n} - n_z\frac{\partial\phi}{\partial s}, \qquad \frac{Dz}{Dt} = \frac{\partial\phi}{\partial z} = n_z\frac{\partial\phi}{\partial n} + n_r\frac{\partial\phi}{\partial s}, \tag{4}$$

and a dynamic boundary condition relating the pressure jump across the capillary interface to the curvature of the interface via

$$\frac{D\phi}{Dt} = \tfrac{1}{2}|\nabla\phi|^2 + \frac{1}{R_1} + \frac{1}{R_2} + p_0 - Bo\,z. \tag{5}$$

In the above equations $D/Dt = \partial/\partial t + (\nabla\phi\cdot\nabla)$ denotes a Lagrangian time derivative, $\boldsymbol{n} = (n_r, n_z)$ is a unit vector normal to the capillary surface and $s$ denotes the arclength along the capillary surface (in the counterclockwise direction). $R_1$ and $R_2$ are the principal radii of curvature of the free surface, $p_0$ is a pressure constant which is defined by the equations governing the static surface and the dimensionless Bond number $Bo = \rho gR^2/\sigma$ is a measure of the ratio of gravitational and surface tension forces. The unit normals and the radii of curvature, expressed explicitly in terms of quantities only defined in the capillary surface, are give by

$$\left.\begin{aligned} n_r &= \frac{z_s}{(r_s^2+z_s^2)^{\frac{1}{2}}}, \quad n_z = \frac{-r_s}{(r_s^2+z_s^2)^{\frac{1}{2}}}, \\ \frac{1}{R_1}+\frac{1}{R_2} &= \frac{z_s r_{ss} - r_s z_{ss}}{(r_s^2+z_s^2)^{\frac{3}{2}}} - \frac{z_s}{r(r_s^2+z_s^2)^{\frac{1}{2}}}, \end{aligned}\right\} \tag{6}$$

in which the subscript $s$ denotes a derivative with respect to the arclength coordinate $s$.

To complete the description of the problem we require a suitable set of initial conditions. We assume that at $t = 0$ the fluid is at rest. The free surface is situated at the mouth of the nozzle (at $z = 1$) and is assumed to be flat. These assumptions determine $p_0$ in (5) via $p_0 = Bo$. For $t > 0$ we assume that the fluid enters the nozzle at $z = 0$ with the velocity given by (3). One could argue that these initial conditions are unphysical in that an infinite acceleration is required at $t = 0$ in order to obtain a constant mass flux for $t > 0$. However, the initial conditions can also be viewed in the following way. Assume that for $t < 0$ a flat capillary surface advances through a cylindrical tube and that the capillary surface reaches the end of the tube at $t = 0$. In this case it is, of course, debatable to what extend the assumption that the capillary surface is flat at $t = 0$ is valid. Indeed, this assumption is likely to be invalid in most practical situations, see e.g. Dussan V., Ramé & Garoff (1991). There are, however, many unanswered questions related to the problem of a capillary surface rising in a tube, the shape of the surface being one. A detailed discussion of this problem is beyond the scope of this paper and the assumption of a flat initial surface should be regarded as a first-order approximation.

It is well-known (cf. Dommermuth & Yue 1987) that finding the solution of the problem defined by (1) subject to the boundary conditions (2) and (3) is equivalent to solving the integral equation

$$\alpha\phi(\boldsymbol{x}) + \int_{\partial\Omega} \phi(\boldsymbol{x}') \frac{\partial G}{\partial n'}(\boldsymbol{x}, \boldsymbol{x}')\, r'\, \mathrm{d}s(\boldsymbol{x}') = \int_S \psi(\boldsymbol{x}')\, G(\boldsymbol{x}, \boldsymbol{x}')\, r'\, \mathrm{d}s(\boldsymbol{x}') + We^{\frac{1}{2}} \int_\Gamma \Psi(\boldsymbol{x}')\, G(\boldsymbol{x}, \boldsymbol{x}')\, r'\, \mathrm{d}s(\boldsymbol{x}'), \quad (7)$$

in which we use the notation $\psi = \partial\phi/\partial n$, and $G(\boldsymbol{x}, \boldsymbol{x}')$ denotes the Green's function for the Laplace equation in cylindrical coordinates,

$$G(\boldsymbol{x}, \boldsymbol{x}') = \frac{4}{\rho_+} K(m), \quad \boldsymbol{x} = (r, z), \quad \boldsymbol{x}' = (r', z'),$$
$$\rho_\pm = [(r \pm r')^2 + (z - z')^2]^{\frac{1}{2}}, \quad m = 1 - \rho_-^2/\rho_+^2,$$

with $K(m)$ denoting the elliptic integral of the first kind. The first integral in (7) is understood in the sense of the Cauchy principal value and the parameter $\alpha$ in (7) is the solid angle at the point $\boldsymbol{x}$ on the boundary subtended by the fluid domain.

## 3. Numerical approximation

In order to obtain a discrete set of equations we divide the boundary of $\Omega(t)$ into $N$ elements. On each element the velocity potential and the flux are approximated by linear interpolating functions. Thus, for the potential on element $e_j$ with nodes $\boldsymbol{x}_j$ and $\boldsymbol{x}_{j+1}$ and $\phi(\boldsymbol{x}_j) = \phi_j$ we take

$$\phi_{e_j}(\xi) = \phi_j \lambda_j^{(1)}(\xi) + \phi_{j+1} \lambda_j^{(2)}(\xi),$$
$$\lambda_j^{(1)}(\xi) = 1 - \xi, \quad \lambda_j^{(2)}(\xi), \quad \xi \in [0, 1],$$

and likewise for the fluxes. Substituting the approximations for $\phi$ and $\psi$ as given above into the integral equation (7) and defining matrix elements via

$$H_{ij} = \int_{e_{j-1}} \lambda_{j-1}^{(2)}(\xi) \frac{\partial G}{\partial n}(\boldsymbol{x}(\xi), \boldsymbol{x}_i)\, r(\xi)\, \mathrm{d}s(\xi) + \int_{e_j} \lambda_j^{(1)}(\xi) \frac{\partial G}{\partial n}(\boldsymbol{x}(\xi), \boldsymbol{x}_i)\, r(\xi)\, \mathrm{d}s(\xi),$$

and $$G_{ij} = \int_{e_{j-1}} \lambda_{j-1}^{(2)}(\xi)\, G(\boldsymbol{x}(\xi), \boldsymbol{x}_i)\, r(\xi)\, \mathrm{d}s(\xi) + \int_{e_j} \lambda_j^{(1)}(\xi)\, G(\boldsymbol{x}(\xi), \boldsymbol{x}_i)\, r(\xi)\, \mathrm{d}s(\xi),$$

it follows that the discrete equivalent of the integral equation (7) is given by

$$\sum_{i=1}^{N} H_{ij}\phi_j = \sum_{i=1}^{N} G_{ij}\psi_j, \quad j = 1, \ldots, N. \tag{8}$$

The integrals for the elements $H_{ij}$, $G_{ij}$ $(i \neq j)$ are regular and are evaluated using a standard four-point Gauss interpolation formula. The elliptic functions in the integrands are evaluated using polynomial approximations given by Abramowitz & Stegun (1972). The integrands in the integrals for the elements $G_{ii}$ contain logarithmic singularities. These integrals are evaluated using a special four-point Gauss formula for integrals with logarithmic singularities. The diagonal elements $H_{ii}$ (corresponding to the singular points in the integrand) are calculated indirectly in the following way. If the potential is constant throughout $\Omega(t)$ then $\psi = 0$. From (8) it follows that for any constant potential we require

$$\sum_{i=1}^{N} H_{ij}\phi_j = 0.$$

In particular, taking $\phi_j = 1$ it follows that the diagonal elements are given by

$$H_{ii} = -\sum_{\substack{j=1 \\ i \neq j}}^{N} H_{ij}.$$

Without elaborating we point out that on the capillary surface the fluxes are unknown while on the nozzle inlet and the nozzle wall the potentials are unknown. This implies that columns of matrices $\boldsymbol{G}$ and $\boldsymbol{H}$ in (8) have to be rearranged in order to bring all the unknowns to one side of the equation. Note also that columns in $\boldsymbol{G}$ that refer to the nodes on the side of the nozzle for which $\psi = 0$ need not be calculated.

Let us next consider the dynamic and kinematic boundary conditions on the capillary surface. The unit normals and the curvatures at node $\boldsymbol{x}_i$, say, are calculated by fitting a locally quadratic spline through $\boldsymbol{x}_i$ and its neighbouring points,

$$\boldsymbol{x}(\xi) = \lambda^{(1)}(\xi)\, \boldsymbol{x}_{i-1} + \lambda^{(2)}(\xi)\, \boldsymbol{x}_i + \lambda^{(3)}(\xi)\, \boldsymbol{x}_{i+1}, \tag{9}$$

in which

$$\lambda^{(1)}(\xi) = \tfrac{1}{2}\xi(\xi-1), \quad \lambda^{(2)}(\xi) = 1-\xi^2, \quad \lambda^{(3)}(\xi) = \tfrac{1}{2}\xi(\xi+1), \quad \xi \in [-1, 1].$$

Using (9) we get for example

$$\left.\frac{\mathrm{d}r}{\mathrm{d}s}\right|_{x=x_i} = \left.\frac{\mathrm{d}r}{\mathrm{d}\xi}\frac{\mathrm{d}\xi}{\mathrm{d}s}\right|_{x=x_i} = J_i \tfrac{1}{2}(r_{i+1} - r_{i-1}),$$

where $J_i = (\mathrm{d}\xi/\mathrm{d}s)|_{x=x_i}$ is the Jacobian, which we assume constant. Similar results hold for $z_s$, $r_{ss}$ and $z_{ss}$. At the point at which the free surface intersects the symmetry axis we have the conditions $z_s = 0$, $r_s = -1$ so that $n_r = 0$ and $n_z = 1$. At this point the principal radii of curvature are identical, i.e. $R_1 = R_2$ and $z_{ss}$ is calculated using symmetry considerations. Finally, to evaluate the tangential derivative $\partial\phi/\partial s$ at node $i$, say, we fit a locally quadratic spline through $\phi_i$ and its neighbours, similar to (9). Note that $\partial\phi/\partial s = 0$ on the symmetry axis.

After having applied the discretization procedure as outlined above, the conditions on the capillary surface can be written as

$$\frac{\mathrm{D}r}{\mathrm{D}t} = f_1(\phi, \psi, r, z), \quad \frac{\mathrm{D}z}{\mathrm{D}t} = f_2(\phi, \psi, r, z), \quad \frac{\mathrm{D}\phi}{\mathrm{D}t} = f_3(\phi, \psi, r, z), \tag{10}$$

in which $f_1, f_2$ and $f_3$ are in general nonlinear functions of their arguments. Together with suitable initial conditions, (10) constitutes an initial-value problem where the relation between $\phi$ and $\psi$ is provided by the discretized integral equation (8),

$$\boldsymbol{H}\boldsymbol{\phi} = \boldsymbol{G}\boldsymbol{\psi}. \tag{11}$$

In (10) and (11) the bold, lower-case quantities refer to vectors, the elements of which refer to variables at the nodal points.

## 4. Time stepping and regridding

In the next section we present results that assume a constant mass flux through the nozzle. The volume enclosed by the capillary surface is therefore proportional to $t$ and hence the area of the capillary surface is proportional to $t^{\frac{2}{3}}$. This implies that, given an initial distribution of nodes, the average distance between two nodes increases steadily. It turns out that the evolution of the capillary surface is by no means uniform. We find that there are regions on the capillary surface in which the flow is largely divergent while other regions exist in which the flow is predominantly convergent. This leads to large variations in the movement of Lagrangian nodes with the effect that some regions of the free surface become severely depleted of nodes while other regions have a large concentration.

The uneven distributions of Lagrangian nodes has two undesirable effects. First, the regions that are depleted of nodes can have significant curvatures. This means that large discretization errors are introduced in the calculation of the unit normals and curvatures. Secondly, like in many previous studies, we find short-wavelength instabilities in regions with a large concentration of Lagrangian nodes. These two points force us to consider some sort of regridding procedure.

Before we proceed with a detailed discussion of the regridding procedure, let us first discuss the implications of regridding on the choice of the time-integration scheme. With regridding it is not desirable to employ multi-step schemes. Namely, the use of multi-step schemes would require extensive use of interpolations in order to determine the 'true' position of the Lagrangian node at the new time level. These interpolations introduce extra discretization errors, in particular when higher-level schemes are used. Single-step schemes are clearly advantageous, although somewhat more expensive due to the increased number of function evaluations required as compared with multi-step schemes of the same accuracy. In our calculations we have employed a slight modified fourth-order Runge–Kutta scheme. The modification consists of the assumption that the matrices $\boldsymbol{G}$ and $\boldsymbol{H}$ in (11) are constant during one complete time step. At the cost of some loss of accuracy during the time integration, this assumption leads to significant savings in computer time, which is dominated by the calculation of the matrix coefficients. Dommermuth & Yue (1987) have used a similar approximation in their calculations.

The Runge–Kutta scheme is not unconditionally stable. For the problem under consideration the stability condition is of the form

$$\Delta t \lesssim O(\Delta x_{min}^{\frac{3}{2}}), \tag{12}$$

where $\Delta x_{min}$ is the minimum distance between any two adjacent nodes on the free surface. This condition follows from the well-known stability criterion for a fourth-order Runge–Kutta scheme, $\Delta t \leqslant \sqrt{8}/\omega$ ($\omega$ being the maximum frequency in the problem under consideration), and the fact that waves dominated by capillary effects typically have frequencies which are of the order $k^{\frac{3}{2}}$, where $k$ denotes the wavenumber ($k_{max} \sim 1/\Delta x_{min}$).

Let us return to the problem of regridding. The stability condition (12) requires that, whatever regridding strategy we choose, for a given time step $\Delta t$ the minimum distance between Lagrangian nodes should be bounded below. Since we do not know in general what the lower bound is, it seems natural to take the lower bound to be the minimum distance between any two adjacent nodes of the initial distribution (assuming that the time step is sufficiently small for stable integration with the initial distribution). This procedure ensures that the stability condition (12) will not be violated during the time integration. During the time integration the distribution of nodes is modified in the following way. After a given number of time steps the nodes are redistributed over the surface so as to maintain an even distribution of nodes. A node is added to the surface whenever the surface area has increased sufficiently to add an extra node without violating the lower bound of the element size as defined above. Since the CPU time per time step increases rapidly as the number of nodes increases, we have set an upper limit to the total number of nodes (typically $N \sim 120$). Once this upper limit is reached we allow the element size on the free surface to increase while regridding is used to maintain a uniform distribution of nodes on the free surface.

To calculate the position of the new node and the value of the velocity potential at the new node we adopt the following strategy. Given an uneven distribution of nodes at some time during the integration procedure. We calculate new nodal positions such that the distance between the nodes (measured along the connecting line elements) is equal for all nodes. Calculations show, however, that restricting the positioning of new nodes to the line elements connecting the old nodes has a strong stiffening effect and leads to mass loss during the time stepping. This is because the lines joining the new nodes always lie entirely within the fluid domain for a convex surface. To overcome this problem the position of the new node is calculated using locally cubic splines. For example, if a new node is situated between original nodes with vertices $i$ and $i+1$, a locally cubic spline is calculated using the values at the nodes $i-1, \ldots, i+2$. The new node is then moved from the line joining nodes $i$ and $i+1$ to the position on the cubic spline such that the relative distance between the new node and the nodes $i$ and $i+1$ remains unchanged. In all calculations presented henceforth we have updated the mesh after each time step in the way outlined above.

We point out that it is not clear *a priori* which criteria to adopt for the repositioning of the nodes on the surface. While the strategy outlined above proved satisfactory, different approaches are possible. In our calculations the mass loss is not completely eliminated and a criterion for an alternative regridding approach could be to minimize mass loss. An additional concern is the possible dissipation of energy as a results of the regridding operation. In the Appendix we show that while our regridding operation dissipates energy, the energy loss is small on the timescales of interest. Oğuz & Prosperetti (1990*a*) have also employed a regridding approach in which a fixed element length is maintained. In addition they stagger the position of the nodes at alternating time steps. It is not transparent what the advantage is of staggering the nodes since additional damping had to be introduced to maintain stability. It appears that an efficient distribution of nodal points may be obtained by relating the nodal distribution to the curvature of the free surface, cf. Van de Vorst, Mattheij & Kuiken (1992). An

advantage of this approach is that strongly curved regions have a higher concentration of nodes than the regions with a smaller curvature. Stability requires, however, that the smallest element be bounded below, regardless of the distribution of nodes. In addition, calculations in the next section show that physical bifurcations can occur in regions that are not strongly curved. It will be clear that a fine distribution of nodes is required in order to resolve the bifurcation point even when the surface is not strongly curved.

## 5. Discussion and results

Numerical experiments show that for a given Bond number and a given volume flux, the evolution of the capillary surface is remarkably independent of the precise form of $\Psi(r)$. It seems appropriate therefore, to present results in terms of the discharge rate $\mathcal{Q}$, defined via

$$\mathcal{Q} = -2\pi We^{\frac{1}{2}} \int_0^1 \Psi(r) r \, dr. \tag{13}$$

The minus sign indicates that fluid enters the nozzle at $z = 0$. In all the numerical experiments in this section we have taken the flux to be of the form $\Psi(r) = -1$ so that the discharge rate is related to the Weber number via $\mathcal{Q} = \pi We^{\frac{1}{2}}$.

Let us now investigate the evolution of the fountain for different values of the Bond number and the discharge rate $\mathcal{Q}$. In all calculations the nozzle inlet and the side of the nozzle were discretized using four elements of equal size. The initial discretization of the capillary surface consists of 32 equally spaced nodes – the number of nodes on the surface increasing rapidly as time increases. We allow the number of nodes on the free surface to increase until the total number of nodes on the boundary is equal to 120. The time step is fixed during the time integration at $\Delta t = 5 \times 10^{-4}$ whenever $t \in [0, 0.15]$ and $t \geqslant 0.25$, while we take $\Delta t = \frac{5}{3} \times 10^{-4}$ for $t \in (0.15, 0.25)$. The reason for changing the time step is that the free surface accelerates near $t \approx 0.2$ as will become apparent shortly.

First consider the case $Bo = 1.0$. For the discharge rates $\mathcal{Q} = 4, 6$ we have plotted the shapes of the evolving fountain in figure 2($a$, $b$) at the times indicated in the plots. The case $\mathcal{Q} = 4$ results in a slowly evolving fountain as shown in figure 2($a$). Speaking of a fountain in this case is somewhat artificial since the capillary surface clearly evolves as a growing sessile drop at the end of the nozzle. We observe that as the capillary surface emerges from the nozzle the surface is flat near the centre with a small rise of the surface near the rim of the nozzle. The height of the mountain grows and small undulations near the symmetry axis are apparent. The amplitude of these undulations grow, resulting in a trough around the symmetry axis at $t = 0.2$. After the free surface emerges from the trough we observe the evolution of the fountain into a drop which reaches a maximum height above the nozzle near $t = 1.5$. Subsequently the drop starts to sag over the mouth of the nozzle and the calculation has to be terminated when the free surface intersects the side of the nozzle. While dynamic effects are clearly important during the initial phase of the evolution, it seems that after $t = 1.0$ the shape of the growing drop is only slightly modified by dynamic effects. This appears in agreement with what one would expect intuitively. Namely, for small discharge rates one would expect the shape of the drop to be determined mainly by its volume and the Bond number. In that case the shape of the growing drop can be regarded, more or less, as a succession of static drop shapes.

When the discharge rate is increased to $\mathcal{Q} = 6$ (figure 2$b$) the evolution of the

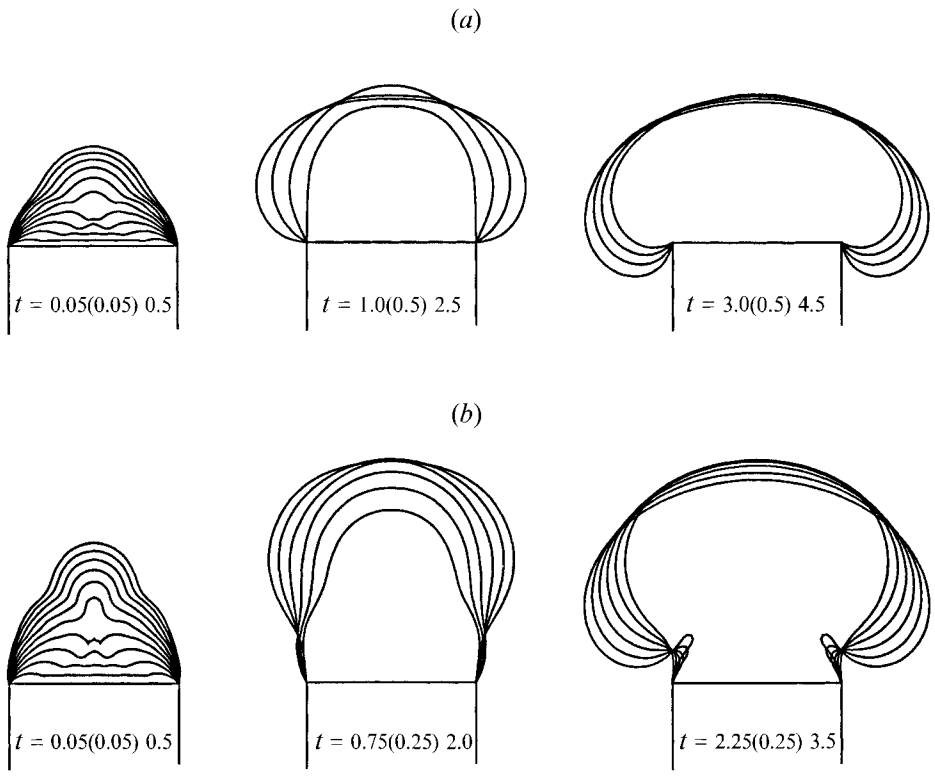


FIGURE 2. Free-surface shapes of an evolving fountain for the parameters $Bo = 1.0$ and (*a*) $\mathcal{Q} = 4$, (*b*) $\mathcal{Q} = 6$. The times are indicated on the plots.

fountain is fundamentally different from that seen in figure 2(*a*). First, we observe that the trough near the symmetry axis has become more localized, with the height of the fountain increasing rapidly as it emerges from the trough. This leads to a pronounced protuberance at the symmetry axis. Subsequently the height of the fountain continues to increase with the fountain assuming a columnar structure. Near $t = 2.0$ the fountain reaches a maximum height after which its head starts to expand. It is interesting to note that as the radius of the head grows, the contribution to the pressure in the head from capillary forces decreases. Hence, whenever capillary forces are important (as is the case when $Bo = 1.0$) the reduction in pressure is significant when the radius of curvature increases. The head will therefore act as a fluid sink, resulting in the increasing growth of the head. We observe that fluid lobes form as a result of the continued growth of the volume of the head. After some time the lobes have grown so much that the free surface folds back onto itself. At this point the calculation has to be terminated. It will be clear that dynamic effects are of major importance with regard to the shape of the evolving fountain. This is in contrast with the observations for $\mathcal{Q} = 4$.

A very interesting change in the evolution of the fountain occurs when for the Bond number $Bo = 1$ the discharge rate is increased to $\mathcal{Q} = 7$. In figure 3 we show the different stages of the evolution of the fountain for these parameters. We observe that during the initial phase of the evolution the dynamic behaviour is very similar to that observed in figure 2(*b*). Namely, the capillary surface is flat near the centre with a small rise of the surface near the rim of the nozzle. Subsequently the height of the rim increases and undulations develop near the centre. We observe that the amplitude of

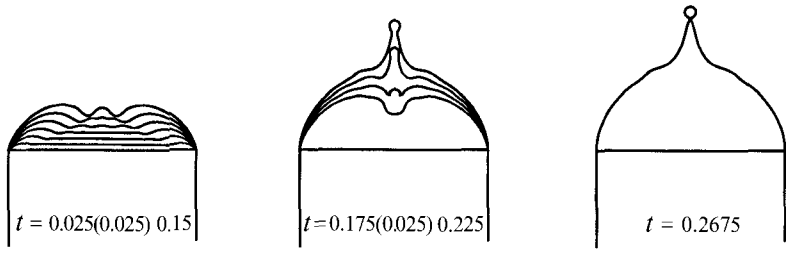


FIGURE 3. Free-surface shapes of an evolving fountain for the parameter values $Bo = 1$ and $\mathcal{Q} = 7$. The times are indicated on the plots.

the undulations increases and a deep trough develops around the symmetry axis. Subsequently, the capillary surface accelerates fast out of the trough resulting in a very large protuberance at the symmetry axis. The tip of the protuberance is rounded and after some time we observe that necking occurs just below the tip of the protuberance, indicating that a drop is formed. Our calculations appear to indicate that the emergence of the capillary surface from the trough is so fast that a drop of fluid is ejected from the free surface.

In order to understand the results of these calculations, it is important to realize that surface tension is the physical effect governing the intricate dynamics of the growing fountain. If surface tension were not present, the fluid region emerging from the nozzle would have sharp edges. Surface tension effects lead to a rounding of the edges, effectively by inhibiting the flow close to the walls of the nozzle. Fluid near the walls of the nozzle is therefore deflected inwards which, together with concervation of mass, results in the rim on the surface seen in figures 2 and 3. As the fluid rim grows and moves inwards we have observed that undulations occur on the free surface near the symmetry axis. These undulations are capillary waves generated by the inward-moving rim. Owing to the rotational symmetry, the amplitudes of the inward moving capillary waves increase as the radius of the wave front shrinks. The result is a large deflection at the symmetry axis, turning into a trough as the rim converges on the symmetry axis. The trough deepens until the action of surface tension forces prevent a further increase in the curvature of the trough. Subsequently fluid is effectively catapulted out of the trough by the action of surface tension forces trying to eliminate regions with a high curvature. The overshoot of this catapulting action is the protuberance at the symmetry axis which is observed in figures 2 and 3. The calculations indicate that the catapulting action can be so strong that a drop is ejected from the capillary surface. The curvature of the trough depends on the discharge rate. It is only above a 'critical discharge rate' that the curvature becomes large enough to accelerate the fluid sufficiently fast in order to eject a drop.

The formation of the trough is intimately linked with the fact that the two timescales that govern the evolution of the fountain become increasingly separated. The inertia timescale, given by $T_I = R/V$ ($V$ being the characteristic velocity), decreases as the discharge rate increases. A 'global' capillary timescale, defined in §2 as $T_C = (\rho R^3/\sigma)^{\frac{1}{2}}$, is essentially constant as long as the typical radius of curvature is of the order of the radius of the nozzle. Hence, if we have $T_C \gg T_I$ (which is equivalent to the condition $We^{\frac{1}{2}} \gg 1$ or $\mathcal{Q} \gg 1$) the evolution of the fountain is fast compared with the capillary scale $T_C$. This means that capillary forces have insufficient time to 'smooth' the free surface and, as a result, large curvatures can develop. Once the localized region with a large curvature has developed, the global capillary timescale is no longer the relevant timescale. A 'local' capillary timescale, with the radius of curvature of the trough as

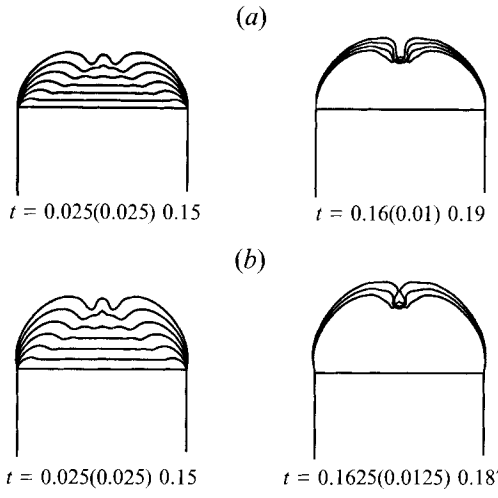


FIGURE 4. Free-surface shapes of an evolving fountain for the parameter values $Bo = 1$ and (*a*) $\mathcal{Q} = 10$, (*b*) $\mathcal{Q} = 14$. The times are indicated on the plots.

the characteristic length, is then the typical timescale on which capillary effects act. This 'local' capillary timescale is much smaller than the 'global' one, reflecting the rapid evolution of the free surface as it emerges from the trough.

When the discharge rate is increased above the critical discharge rate at which bifurcation occurs we find that the trough deepens and the curvature of the trough increases. In figure 4(*a*) we show the evolution of the fountain for the parameters $Bo = 1$ and $\mathcal{Q} = 10$. Often, as in this case, we are not able to continue the numerical integration to the point at which bifurcation occurs after fluid is ejected from the trough. The reason is that as fluid accelerates out of the trough the calculation often breaks down because the first free-surface node after the node already placed on the axis intersects the symmetry axis. This can only be prevented by resorting to excessive smoothing which, of course, also effects the subsequent dynamics. Recall that in none of the calculations presented here explicit smoothing is required.

When the discharge rate is increased further, interesting effects occur. For the parameter values $Bo = 1$ and $\mathcal{Q} = 14$ we observe in figure 4(*b*) that the depth of the trough together with the increased discharge rate leads to the closure of the trough at the top. Apparently the evolution is so fast that capillary forces have insufficient time to catapult fluid out of the trough. This leads to the rather surprising result that for certain discharge rates an air bubble is entrained by the capillary surface. Increasing the discharge rate further is not always clear if an air bubble will be entrained or not since sometimes the calculation breaks down before the capillary surface closes above the trough. However, for discharge rates up to $\mathcal{Q} = 30$ our calculations indicate that air bubbles can be entrained. It is interesting to point out that bubble entrainment by axisymmetric capillary surfaces also occurs in an entirely different context. Namely, if a drop impacts on a liquid surface a bubble may be entrained depending on the impact velocity and the drop diameter, see for example Oğuz & Prosperetti (1990*a*). In order to explain the mechanism leading to the entrainment of the bubble, Oğuz & Prosperetti (1990*b*) suggested that the effect could be due to an axisymmetric wavefront converging on the symmetry axis. Their calculations indicated that this was indeed a possible entrainment mechanism, which is in agreement with our results.

So far we have investigated the evolution of the fountain as a function of the

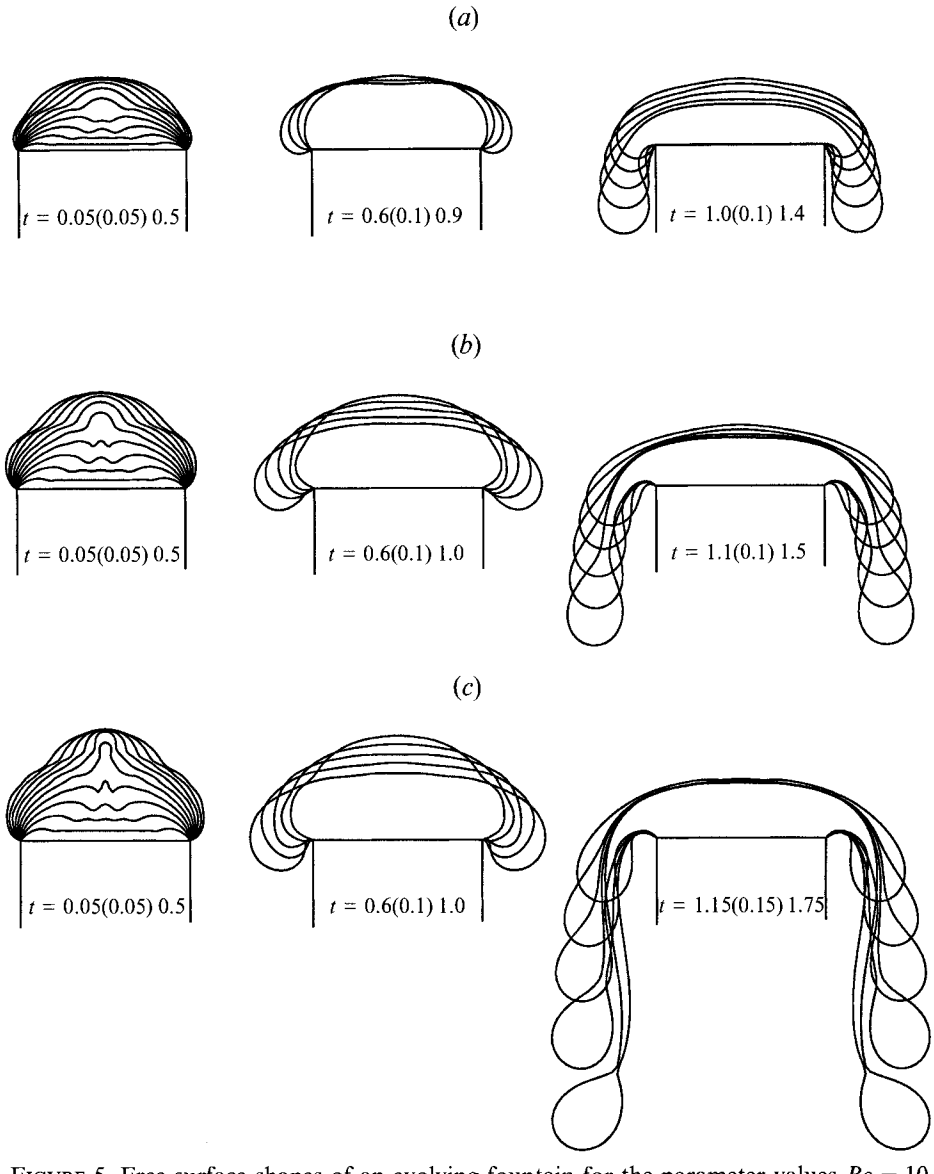


FIGURE 5. Free-surface shapes of an evolving fountain for the parameter values $Bo = 10$ and (*a*) $\mathcal{Q} = 4$, (*b*) $\mathcal{Q} = 6$, (*c*) $\mathcal{Q} = 7$. The times are indicated on the plots.

discharge rate for the Bond number $Bo = 1$. In order to assess the effect of the Bond number we take $Bo = 10$ and again study the evolution of the fountain as a function of the discharge rate. In figure 5(*a–c*) we have plotted the evolution of the fountain for the discharge rates $\mathcal{Q} = 4$, 6 and 7 respectively. We observe that for $\mathcal{Q} = 4$ (figure 5*a*) the initial stage of the evolution is qualitatively the same as that seen in figure 2(*a*). Between $t = 0.5$ and 1.0 in figure 5(*a*) we observe a drop-shaped surface which does not change dramatically. Again we believe that the shape of the drop is mainly determined by the Bond number and the volume of the drop. After $t = 1.0$ we see that the volume of the drop has grown so much that lobes form which fall over the sides of the nozzle. Eventually the lobes intersect the sides of the nozzle at which point the calculation has to be terminated.

When, with $Bo = 10$, the discharge rate is increased to $\mathcal{Q} = 6$ we observe (figure 5*b*) that dynamic effects have a significant effect on the shape of the fountain throughout the evolution. First, we note that the protuberance at the symmetry axis is more pronounced that for $\mathcal{Q} = 4$. We see that the fountain reaches a maximum height near $t = 0.5$ after which the height decreases significantly. The lobes that form fall over the side of the nozzle. The lobes continue to grow with the result that part of the nozzle is momentarily surrounded by a fluid curtain. Eventually the calculation is terminated because the fluid curtain can no longer sustain the weight of the ring of fluid at the bottom of the curtain – a bifurcation occurs in the fluid curtain. An interesting observation is that after a significant decrease, the height of the fountain attains a more or less fixed value. It is clear that the pressure of the flow emerging from the nozzle prevents a further decrease of the height.

Let us next consider the evolution of the fountain for the parameters $Bo = 10$ and $\mathcal{Q} = 7$. Recall that for the same discharge rate and $Bo = 1$ a drop was ejected from the free surface. In figure 5(*c*) the free surface is shown at different stages of the evolution. We note the large protuberance near $t = 0.25$. However, the acceleration is clearly not sufficiently strong to eject a drop from the free surface. The subsequent evolution is very similar to that seen in figure 5(*b*). After reaching a maximum near $t = 0.5$ the height of the fountain decreases significantly as the lobes form. Again we see the formation of a fluid curtain around the nozzle and, eventually, the bifurcation of the fluid curtain.

The foregoing results suggest that increasing the Bond number has a stabilizing effect in the sense that a larger discharge rate is required to yield a bifurcation. This is not unexpected since the capillary surface is flattened by large Bond numbers. While the critical discharge rate, $\mathcal{Q}_{crit}$, increases with increasing Bond number, we find that this increase is only gradual. For example, for $Bo = 10$ we find $\mathcal{Q}_{crit} = 8$, for $Bo = 50$ we find $\mathcal{Q}_{crit} = 9$ and for $Bo = 100$ the critical discharge rate is $\mathcal{Q}_{crit} = 13$. Increasing the discharge rate beyond $\mathcal{Q}_{crit}$ we find that an air bubble may be entrained for a sufficiently small Bond number. Only for Bond numbers less than 30 did we observe entrainment of a bubble, for larger Bond numbers entrainment was never observed. As was pointed out before, owing to numerical difficulties it was often not possible to establish beyond doubt whether entrainment would occur. It is important to realize that these numerical difficulties may indicate very violent physical effects. It is for example, not at all clear what would happen physically if the top of the trough were to close just at the point at which the bottom of the trough is accelerating upwards.

It turns out that interesting information regarding the dynamics of the evolving fountain can be obtained by considering its height as a function of time for different parameters. We define the height $H$ of the fountain to be the height of the capillary surface at the symmetry axis measured from the mouth of the nozzle. For the discharge rates $\mathcal{Q} = 3, 5, 7, 9$ and the Bond numbers $Bo = 1$ (solid lines) and $Bo = 10$ (dotted lines), figure 6 shows graphs of the height of the fountain as a function of time. There are a number of interesting points to note. First, we observe that during the initial stage of the evolution the height of the fountain is not affected by the Bond number. Only after $t = 0.2$ do we observe that the effect of increasing the Bond number is to decrease the maximum height attained by the fountain. Up to $t = 0.1$ the height of the fountain increases linearly with time with no dependence on the Bond number. To a very good approximation the height of the fountain up to $t = 0.1$ is given by $H(t) = \mathcal{Q}t/2.91$ which is somewhat higher than the value $H(t) = \mathcal{Q}t/\pi$ that one would get if the fountain would emerge from the nozzle as a perfect cylinder with sharp edges.

The oscillatory increase of the height between $t = 0.1$ and 0.2 is due to the

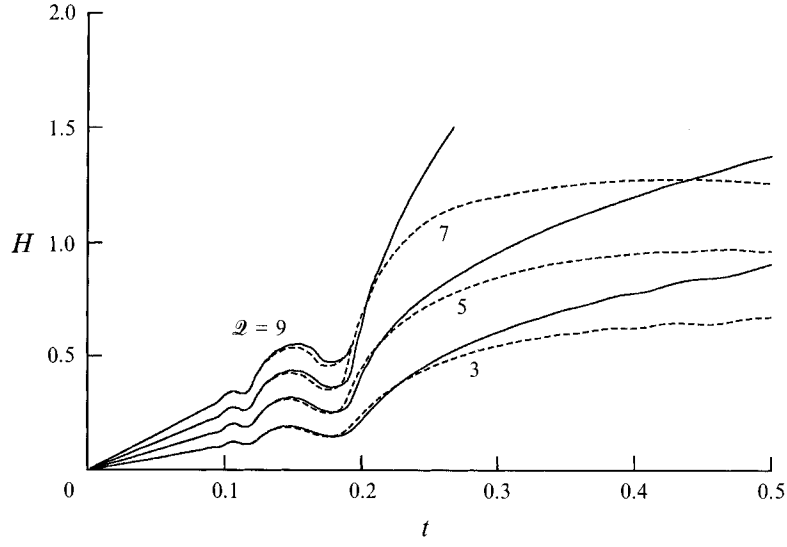


FIGURE 6. The height $H$ of the fountain above the nozzle versus time for the discharge rates $\mathcal{Q} = 3, 5, 7, 9$ and the Bond numbers $Bo = 1.0$ (solid line) and $Bo = 10$ (dotted lines).

convergence on the symmetry axis of the concentric capillary waves propagating in advance of the fluid rim as seen in figures 2–5. The amplitudes of the oscillations increase and just before $t = 0.2$ we observe a significant decrease in the height of the fountain at the symmetry axis, being the point at which the trough develops. Subsequently the height at the symmetry axis increases rapidly as the surface accelerates upwards out of the trough. The calculation is terminated due to the ejection of a drop when $Bo = 1$ and $\mathcal{Q} = 7$ or due to the intersection with the symmetry axis of free-surface nodes in the trough when $\mathcal{Q} = 9$ and $Bo = 1, 10$.

For the discharge rate $\mathcal{Q} = 3$ we observe that after the fairly rapid increase $t = 0.2$ the height of the fountain increases slowly in an oscillatory manner. It appears that the rapid transition caused by the fluid emerging from the trough excites an eigenmode of the growing fountain. As was evident from the plots in figures 2(*a*) and 5(*a*), the fountain evolves slowly as a sessile drop when $\mathcal{Q} = 4$. While the eigenvalues of the growing drop are time dependent, an eigenmode may be excited when the variation of the eigenvalues with time is small enough. The oscillatory growth is also apparent in figure 5(*a*) at the times $0.5 \leqslant t \leqslant 1.0$. We observe that for the larger discharge rates no clear oscillatory behaviour is present. The reason is that for the larger discharge rates the eigenfrequencies of the fountain change too fast for an eigenmode to be excited.

Let us next investigate in some detail the maximum height attained by the fountain. As was clear from figures 2 and 5, the height of the fountain varies significantly with the discharge rate and the Bond number. In all cases presented we see that the height of the fountain increases, reaches a well-defined maximum and subsequently decreases before the calculation breaks down. We have plotted the maximum height $H_{max}$ as a function of the discharge rate $\mathcal{Q}$ for different values of the Bond number in figure 7. We observe that for small values of the $\mathcal{Q}$ ($\mathcal{Q} \leqslant 4$) the maximum height of the fountain is virtually independent of the discharge rate. The reason for this behaviour, as explained earlier, is that when $\mathcal{Q}$ is small the shape of the fountain is essentially a sessile drop which grows slowly at the mouth of the nozzle (cf. figures 2*a* and 5*a*). The shape of the growing drop is mainly determined by its volume and by the balance between

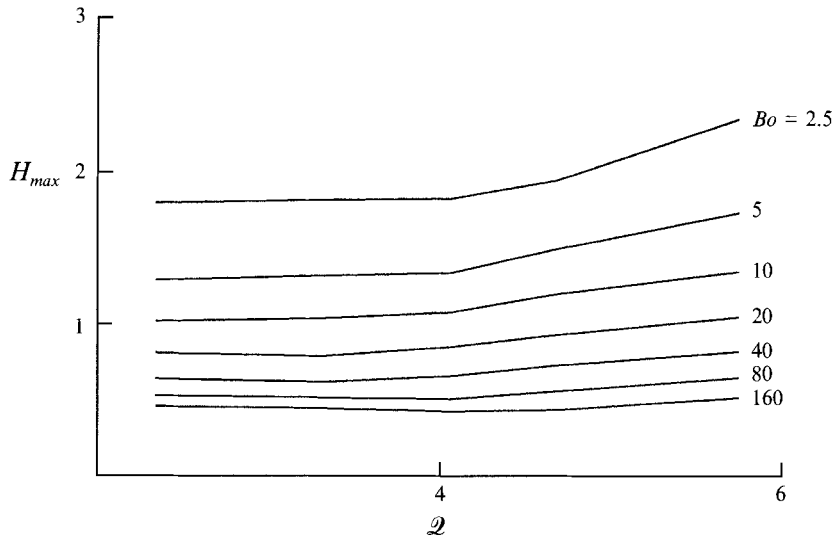


FIGURE 7. A $H_{max}$ versus $\mathcal{Q}$ for the Bond numbers indicated.

surface tension and gravitational forces while dynamic effects are small. Increasing the discharge rate beyond $\mathcal{Q} = 4$ we see that the maximum height increases with increasing discharge rate.

From the foregoing discussion, in which we have considered the evolution of the fountain for different values of the parameters $Bo$ and $\mathcal{Q}$, it emerges that four evolution regimes may be identified. The parameter range in which each of the four evolution patterns exists has been determined by means of numerical experiments. Figure 8 shows the four different regimes in the ($\mathcal{Q}$, $Bo$)-plane. For small discharge rates ($\mathcal{Q} \leqslant 4$, regime I) the fountain is more accurately described by a sessile drop which sags over the side of the nozzle as the volume of the drop increases. Dynamic effects are of minor importance during a significant part of the evolution: the shape of the drop is largely determined by its volume and the Bond number. Regime I can therefore be referred to as the quasi-static regime. The most important characteristic of regime I is that the maximum height attained by the fountain is independent of the discharge rate (cf. figure 7). Examples of fountains in this regime are given in figures 2(*a*) and 5(*a*).

When dynamic effects become important ($\mathcal{Q} > 4$) three different regimes may be identified. In regime II dynamic effects are important while the discharge rate is below the critical discharge rate. For small Bond numbers regime II is characterized by the evolution of the fountain into a mushroom-like configuration with the head of the fountain folding onto the column supporting the head (cf. figure 2*b*). For larger Bond numbers the evolution in regime II is characterized by a significant decrease of the height of the fountain after the maximum height has been attained. Fluid falls over the side of the nozzle resulting in a fluid curtain surrounding the nozzle (cf. figure 5*b*,*c*). Regime III is characterized by the ejection of a drop from the free surface (cf. figure 3). The critical discharge rate increases with increasing Bond number. For still larger discharge rates (regime IV) we find that an air bubble may be entrained by the capillary surface when the Bond number is sufficiently small (cf. figure 4*b*).

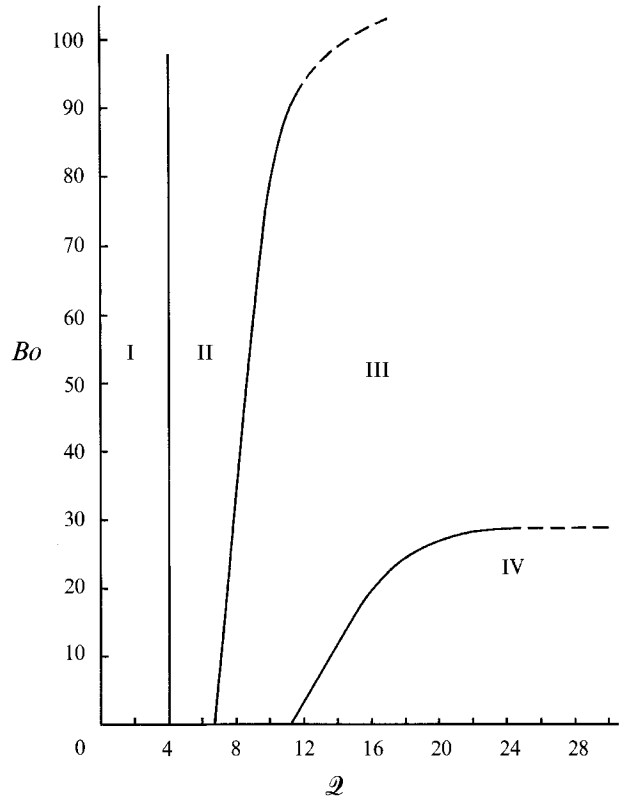


FIGURE 8. Four identifiable regimes in the dynamics of evolving capillary fountains. The different regimes are explained in the text.

## 6. Experimental results

In order to verify some of our numerical results some simple experiments were carried out. A number of stainless steel nozzles were constructed, each 6 cm long with diameters equal to $R = 5, 8, 10$ and 12 mm. The end of each nozzle through which fluid was ejected was tapered to produce a razor-sharp rim. Prior to an experiment, the nozzles were cleaned thoroughly (with trichloro-trifluoro-ethane), carefully levelled and connected through a plastic tube (approximately 40 cm long) with a 12 V washerpump. In all the experiments de-ionised water was used as the working fluid. We assume a value for the surface tension coefficient of $\sigma = 7.2 \times 10^{-2}$ N m$^{-1}$ which corresponds to that of a pure air–water interface. Since purified water is highly prone to contamination by organic materials this value of $\sigma$ should, however, be regarded as only a rough approximation to the true value. With this value of the surface tension coefficient it follows that the Bond numbers corresponding to the different nozzles are equal to $Bo = 0.85, 2.2, 3.4, 4.9$.

An obvious difficulty one encounters in the experiments is how to obtain initial conditions that are as close as possible to the initial conditions employed in the numerical work. There we assumed that at some time $t = 0$ the free surface was flat and positioned at the mouth of the nozzle. For $t > 0$ fluid was ejected from the nozzle at a constant rate. In order to obtain this situation in practice one would require a pump that accelerates the fluid on a timescale small compared with the capillary timescale

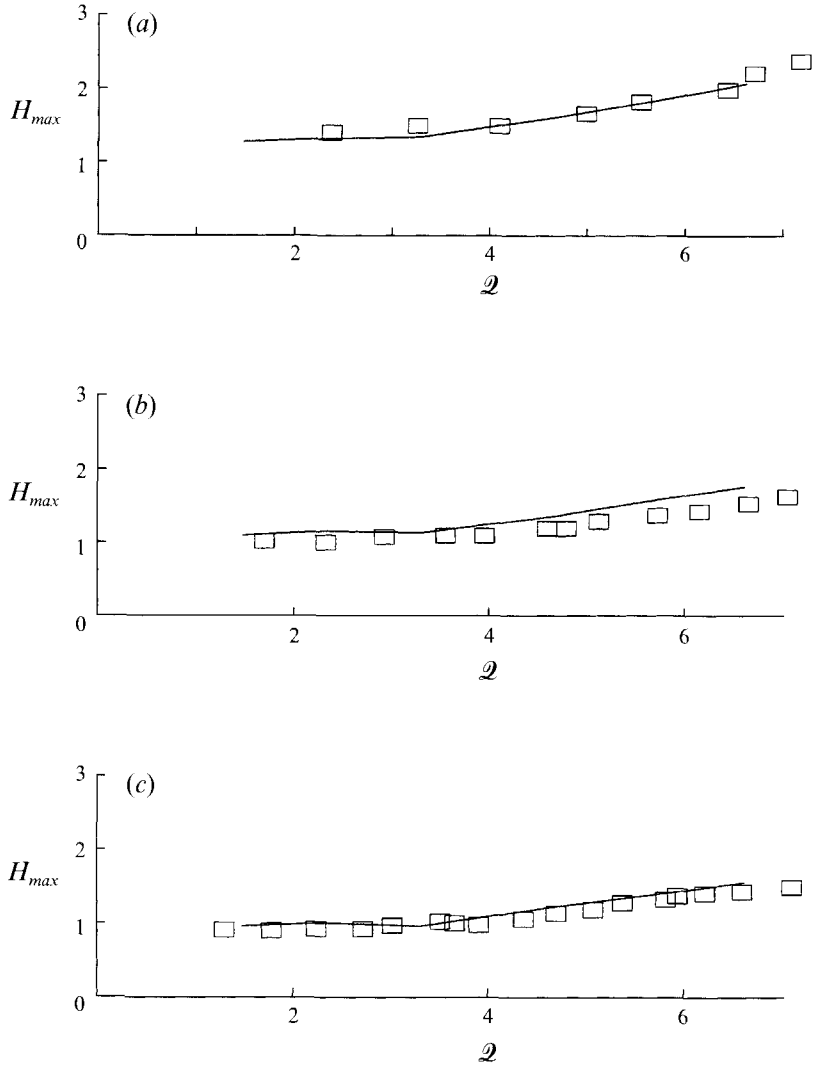


FIGURE 9. The maximum height $H_{max}$ attained by the fountain as a function of the discharge rate. The symbols correspond to the experimental results, the line is the numerical result. (*a*) $Bo = 2.2$, (*b*) $Bo = 3.4$, (*c*) $Bo = 4.9$.

$(\rho R^3/\sigma)^{\frac{1}{2}}$. For nozzles with a radius of approximately 0.5 cm the capillary timescale is of the order of $10^{-2}$ s. Accelerating fluid in a fraction of this time is however not possible with the pump we used. To overcome this problem we opted to allow the fluid to accelerate by switching on the pump when the fluid surface was approximately 5 cm below the mouth of the nozzle. By measuring the height attained by the fountain, we found that the maximum height was independent of the distance of the initial fluid surface below the mouth of the nozzle provided this distance was larger than approximately 4 cm. This suggests that a distance of 5 cm is sufficient to accelerate the fluid with the pump we used. Note that allowing the fluid to advance through the nozzle leads to the difficulty pointed out earlier: the shape of an advancing capillary surface in a nozzle is not horizontal when it leaves the mouth of the nozzle. An additional difficulty with the advancing capillary surface in the nozzle is that the

symmetry is often lost due to the uneven advance of the contact line. The best remedy for this problem was to wet the inside of the nozzle by switching the pump on and off immediately prior to an experiment. Then, after the fluid surface had retreated to its starting level, the pump was switched on for the experiment. While this procedure lead to a significant improvement, asymmetries were still not completely eliminated in most experiments.

As a test of our numerical work it is interesting to see if our prediction that, for small discharge rates, dynamic effects are of minor importance in relation to the shape of the fountain is confirmed in experiments. For the smallest nozzle with corresponding Bond number $Bo = 0.85$ symmetry of the fountain was generally lost before the maximum height was attained. In addition, it was hard to control small volume fluxes (such as $\mathcal{Q} \leqslant 6$ for a 2.5 mm nozzle). For the three larger nozzles the fountain did reach a well-defined maximum before symmetry was lost. In figure 9(*a–c*) we show the maximum height attained by the fountain as a function of the discharge rate for the Bond numbers $Bo = 2.2, 3.4$ and 4.9 respectively. The line represents the numerical solution and the symbols are the experimental results. The sizes of the symbols are approximately equal to the experimental errors. We observe that the numerical results agree reasonably well with the experimental values. Note in particular that the maximum height is virtually independent of the discharge rate when $\mathcal{Q} \leqslant 4$, which is in agreement with our classification depicted in figure 8.

For large discharge rates dynamic effects are important and some interesting phenomena can be observed. Examples of the evolution of the capillary fountain as observed in experiments are shown in figure 10. The different images are selected frames from a high-speed film taken at 250 frames $s^{-1}$. The time separation of the frames is indicated in the figure caption. We note that in all cases presented in figure 10(*a—d*) the discharge rate is such that on the basis of our numerical work we would have expected signs of the ejection of a drop or the entrainment of an air bubble. This is however not what is observed. We will return to this point later.

Let us first consider figure 10(*a*) ($Bo = 0.85$, $\mathcal{Q} = 14.1 \pm 0.4$). We observe that a more or less symmetric capillary surface emerges from the nozzle. The height of the fountain increases fast and after some time (the fourth frame) a neck starts to develop on the liquid column. As this neck moves downwards towards to mouth of the nozzle the radius of the neck decreases. In the last frame we observe that the neck is situated just above the mouth of the nozzle and the fountain starts to lose its symmetric shape. The smaller curvature at the head of the fountain is the reason why the necking region is not advected with the fluid but, instead, moves upstream towards to nozzle mouth. Namely, the smaller curvature of the head means that the capillary pressure in the head is less than that in the column supporting the head and hence the head acts as a fluid sink. As the head grows the capillary pressure decreases and consequently fluid is 'sucked' out of the column causing the neck to move downwards.

In figure 10(*b*) we observe the evolution of the fountain for the parameters $Bo = 2.2$ and $\mathcal{Q} = 10.9 \pm 0.3$. In the first frame we see a large (not quite symmetric) protuberance near the symmetry axis which is similar to what was seen in the numerical work. The protuberance is the signature of a region with large curvature which must have developed near the symmetry axis shortly beforehand. However, no drop is ejected from the surface. We observe that the fountain evolves into a mushroom-like configuration. In the penultimate frame there is evidence that the free surface of the head folds over the column supporting the head (note the sharp transition between the head and the column). This is, in a way, similar to what was seen in the numerical calculation with $Bo = 1$ and $\mathcal{Q} = 6$ (figure 2*b*). In the last frame of figure 10(*b*) we see

(*a*)

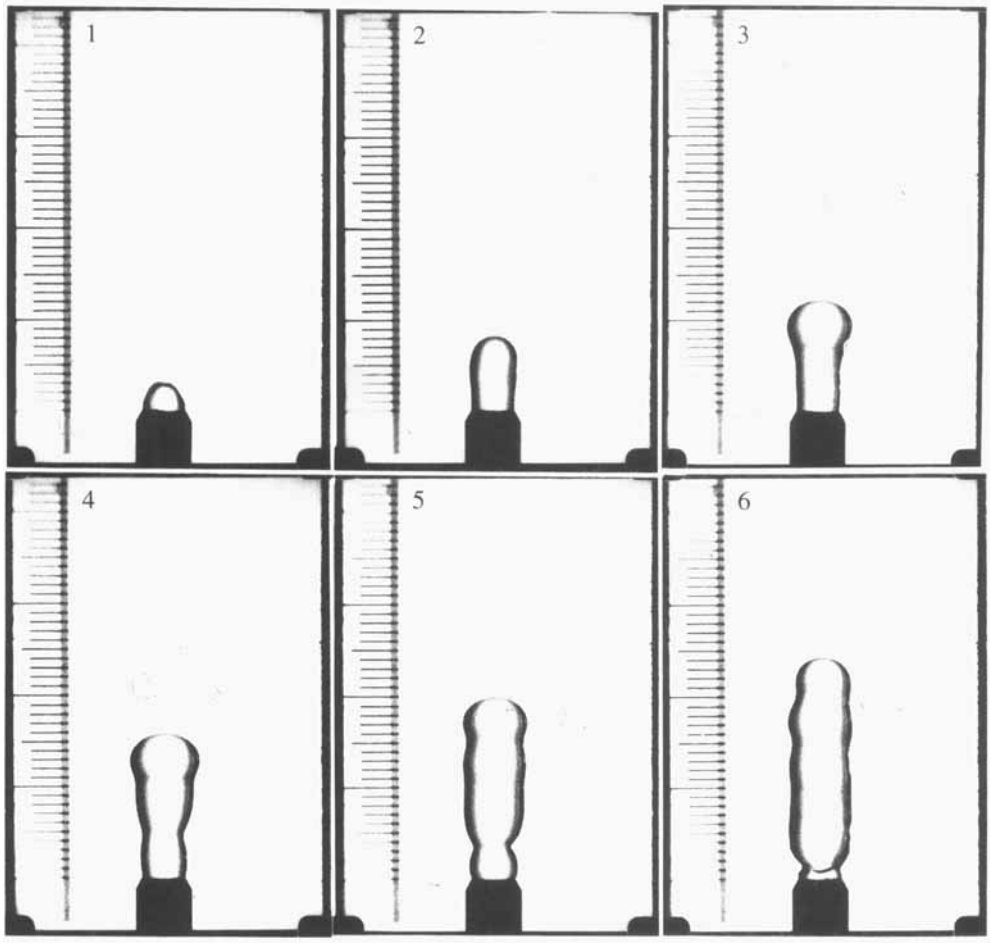


FIGURE 10(*a*). For caption see p. 245.

that the loss of symmetry occurs at the head, presumably because the surface of the head folds onto the column. Any small asymmetry will be magnified very fast at that point.

Figure 10(*c*) shows the evolution of the fountain for the parameters $Bo = 2.2$ and $\mathcal{Q} = 24.3 \pm 0.2$. The rapid evolution is initially very similar to that seen in figure 10(*a*) with the exception that the head is more pronounced in the present case. The subsequent development is, however, markedly different. In the last three frames of figure 10(*c*) we observe that undulations develop on the column supporting the head. The wavelength of the undulation appears more or less constant. The column collapses when the amplitude of the undulation has grown beyond a critical level. It is not obvious what mechanism leads to the formation of these undulations. It could be that a longitudinal-type oscillation is excited in the fountain or the effect may be related to the buckling of the column under the weight of the head.

Finally, in figure 10(*d*) the evolution of the fountain is shown when $Bo = 3.4$ and $\mathcal{Q} = 11.3 \pm 0.1$. We observe the evolution of the fountain into a mushroom-like structure. Evidence that lobes have formed follows from the sharp transition between the

(*b*)

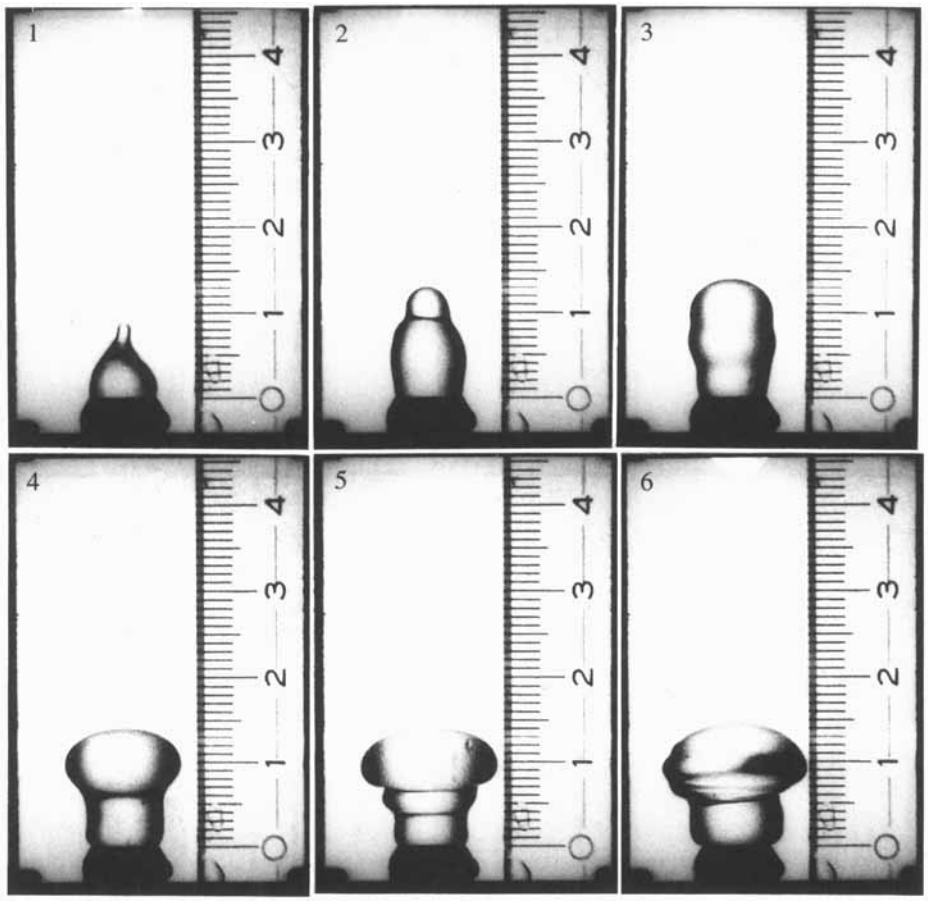


FIGURE 10(*b*). For caption see p. 245.

columnar region and the head as visible in the last frame. The evolution of the fountain with $Bo = 4.9$ and discharge rates in the range $10 \leqslant \mathcal{Q} \leqslant 15$ was very similar to that shown in figure 10(*d*). For smaller discharge rates we typically observed the collapse of the fountain over the rim of the nozzle. With the pump we used we were unable to achieve a discharge rate of $\mathcal{Q} > 20$ for the two largest nozzles. We were therefore unable to determine whether or not the buckling-like behaviour observed in figure 10(*c*) is a persistent feature for larger Bond numbers and large discharge rates.

The most significant discrepancy between numerical and experimental work is that the ejection of a drop is generally not observed experimentally although expected on the basis of our numerical work. The ejection of a drop from the surface shortly after the fountain emerges from the nozzle was never observed in experiments with the 5, 10 and 12 mm nozzles, however, it was observed occasionally with the 8 mm nozzle. In figure 11 we present successive frames of a high-speed film showing the ejection of a drop from the 4 mm nozzle when the discharge rate was $\mathcal{Q} = 13.4 \pm 0.1$. Although the parameter values are different, there is reasonable qualitative agreement between the first frame in figure 11 and the final free-surface shape prior to bifurcation as shown in figure 3. Unfortunately the ejection of the drop is not a persistent feature. It seems

(*c*)

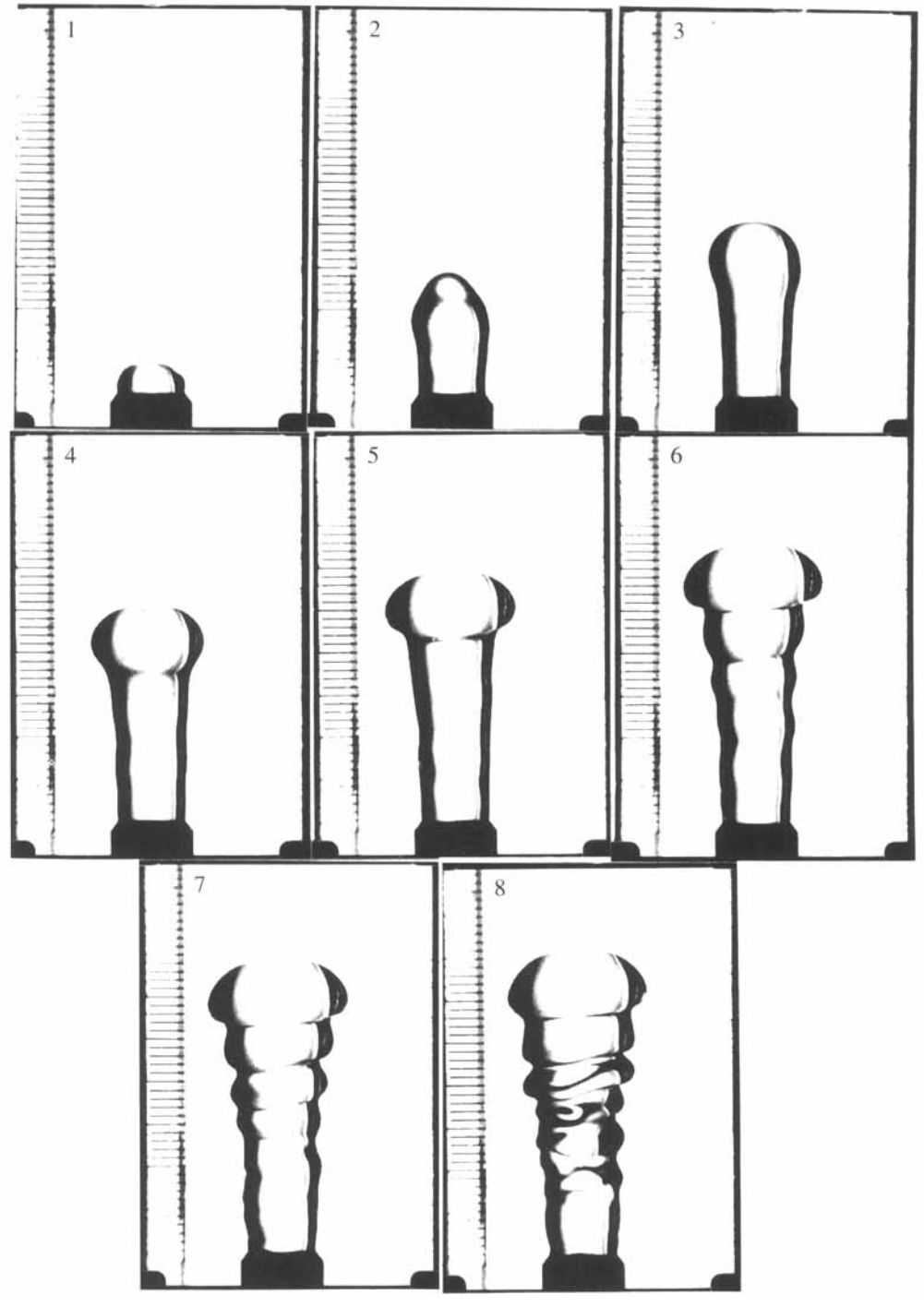


FIGURE 10(*c*). For caption see facing page.

(*d*)

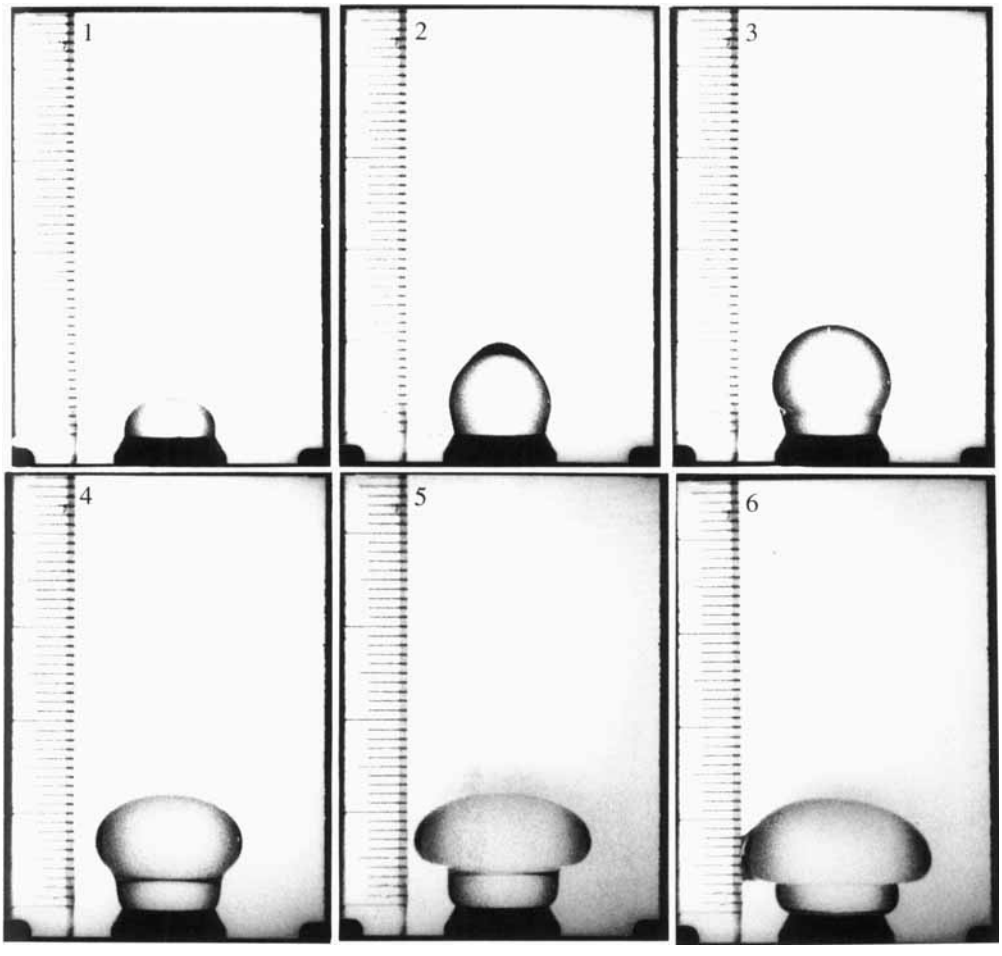


FIGURE 10. Selected frames from a high-speed film (film speed: 250 frames $s^{-1}$): (*a*) $Bo = 0.85$ and $\mathcal{Q} = 14.1 \pm 0.4$, the first two frames are separated 12 ms and the remaining frames by 16 ms. (*b*) $Bo = 2.2$ and $\mathcal{Q} = 10.9 \pm 0.3$, all frames are separated 16 ms. (*c*) $Bo = 2.2$ and $\mathcal{Q} = 24.3 \pm 0.2$ the first six frames are separated 16 ms and the separation of the last three frames is 8 ms. (*d*) $Bo = 3.4$ with $\mathcal{Q} = 11.3 \pm 0.1$, all frames are separated 16 ms. The millimetre markings on a ruler are visible on each frame.

that one of the most important prerequisites for the ejection of the drop is a symmetric surface. The fact that the capillary surface is almost certainly not flat when it emerges from the nozzle will also effect the subsequent dynamics of the fountain but numerical evidence suggests that a drop may be ejected even when the surface is curved (parabolic shape). However, only when the surface is symmetric can we expect the formation of a deep trough at the symmetry axis resulting from the axisymmetric wavefront converging on the symmetry axis. It appears that with the advance of the capillary surface through the nozzle, small asymmetries are generated which prevent the trough being formed. Interesting in this respect is the observation that cleaning the nozzle thoroughly had an adverse effect on the drop formation – no drops were generally observed with a very clean nozzle while drops were observed after the nozzle had been used for some time. This adds to our conviction that the dynamic behaviour of the

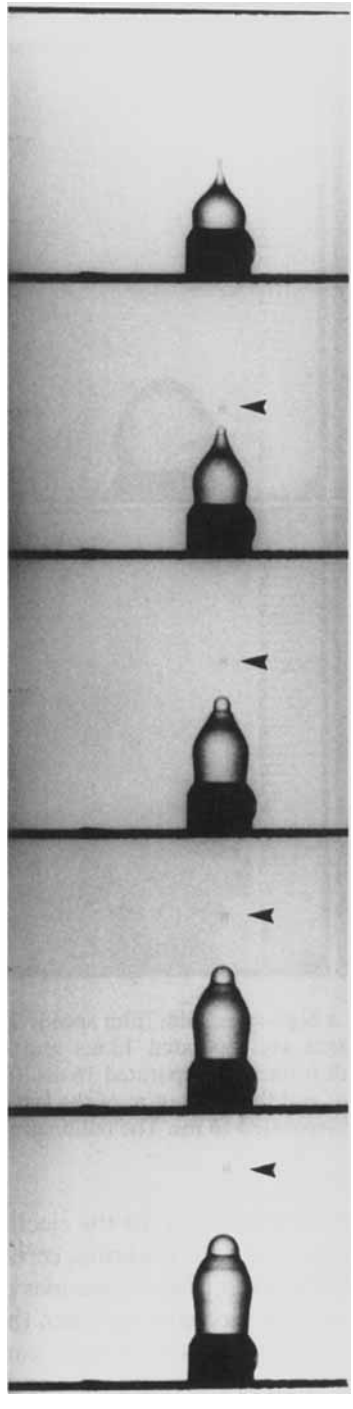

FIGURE 11. The ejection of a drop from the free surface of an evolving fountain. The diameter of the nozzle is 8 mm, the discharge rate is $\mathcal{Q} = 13.4 \pm 0.1$. The frames are 4 ms apart and the arrow indicates the position of the drop.

contact line (which is affected by the cleanliness of the nozzle) is very important. Whenever drops were observed the dimensionless discharge rate was at least 10. Below this value no drops were ever observed. This value is almost 50% higher than what is predicted on the basis of our numerical work. Unfortunately we have insufficient data to make a reliable statement.

On the basis of our numerical work we would also expect an air bubble to be entrained by the capillary surface for a sufficiently large discharge rate. Only on one occasions was an air bubble observed in the head of the fountain. However, even with this bubble we are not entirely certain whether it was the result of entrainment. Unequivocal experimental evidence that an air bubble can be entrained by the capillary surface has yet to be obtained.

It seem appropriate to give an *a posteriori* justification of the potential flow assumption since we compare our numerical work with the experimental results. For small discharge rates ($\mathcal{Q} \leqslant 4$) the velocities are small (typically $v \leqslant 0.2$ m s$^{-1}$ and so the Reynolds number is relatively small, in particular for the smallest nozzle ($Re \leqslant 500$ for the smallest nozzle when $\mathcal{Q} \leqslant 4$). Recall that for small discharge rates dynamic effects are of minor importance since the fountain evolves as a slowly growing drop at the end of the nozzle. Hence the fact that for small discharge rates the potential flow assumptions are not quite justified is compensated by the observation that dynamic effects are of minor importance anyhow. Near the critical discharge rate the Reynolds number for all nozzles is at least 1000. When the discharge rate is large, the main effect of the viscous forces is to modify the velocity profile at the mouth of the nozzle. However, the velocity profile is relatively unimportant as numerical experiments have shown. Hence one is justified in assuming potential flow conditions in the study of water fountains.

## 7. Conclusions

In this paper we have studied the evolution of capillary fountains by employing an integral formulation of the governing equations. Because the area of the capillary surface increases with time, a regridding strategy is applied in which (i) nodal positions are updated so as to maintain a uniform distribution of nodes, and (ii) nodes are added to the free surface to prevent a continuous increase in the average length of elements. With the regridding procedure no short-wavelength instabilities are present during the time integration. When the regridding procedure is applied such that positions of new nodes are restricted to line elements joining old nodes, we find that mass is lost as a result of the regridding operation. In addition, the regridding operation has a significant stiffening effect, in particular close to a bifurcation point. It is found that these problems can be reduced by calculating the new nodal positions using locally cubic splines.

Numerical experiments indicate that four different evolution regimes exist. For small values of the discharge rate ($\mathcal{Q} < 4$) the fountain evolves as a sessile drop at the mouth of the nozzle. Apart from the initial stage of the evolution in which dynamic effects are still important, the shape of the drop is determined mainly by its volume and the Bond number. In addition we find that the maximum height attained by the fountain is independent of the discharge rate when the discharge rate is small. When $\mathcal{Q} > 4$ dynamic effects become important. First, we find that the height attained by the fountain increases with increasing discharge rates. When the discharge rate is below a critical value (which depends on the Bond number) the evolution of the fountain is characterized by the formation of lobes. For small Bond numbers these lobes fold onto

the fluid column supporting the head while for larger Bond numbers the lobes fall over the side of the nozzle thus surrounding the nozzle by a curtain of fluid. Calculations show that eventually this curtain of fluid becomes unstable. For a sufficiently large discharge rate our numerical calculations suggest that a physical bifurcation may occur. This bifurcation is related to the ejection of a drop from the capillary surface. For even larger discharge rates our calculations suggest that an air bubble may be entrained by the capillary surface.

Some simple experiments have been carried out in order to verify some of our numerical predictions. The biggest difficulty we experienced in the experiments is how to bring the initial conditions in the experiment in line with the prescribed initial conditions in the numerical work. A symmetric surface emerging from the nozzle is hard to obtain experimentally. In particular the ejection of a drop from the free surface appears to be affected strongly by small asymmetries. Experiments appear to confirm our numerical prediction that for discharge rates less than $\mathcal{Q} = 4$ the shape of the evolving fountain is mainly determined by the Bond number and the volume rather than dynamic effects.

For large discharge rates interesting phenomena are observed. When the Bond number is small ($Bo = 0.85$) the evolution of the fountain is characterized by a neck which moves towards the mouth of the nozzle. For a larger Bond number ($Bo = 2.2$) the fountain assumes the shape of an extended mushroom rising high above the nozzle while maintaining its symmetry. Subsequently large undulations develop on the liquid column leading to a violent collapse of the fountain.

While the ejection of drops from the free surface has been observed, we have been unable to obtain a good numerical value for the critical discharge rate from our experiments. Neither have we been able to establish unequivocally that an air bubble will be entrained for a sufficiently large discharge rate, as is predicted numerically.

The author is indebted to staff of DAMTP for help and advice in carrying out the experiments. He is also grateful to Janet Ververda for proofreading numerous drafts of this paper. The research was financed by the Commission of European Communities under contract number B/SC1-900617.

## Appendix

Since the numerical scheme outlined in §§ 3 and 4 does not require explicit smoothing to suppress short-wavelength instabilities, the question arises of whether the regridding procedure we have used dissipates energy excessively. In order to answer this question we study the following test problem. A cylindrical container with unit radius and unit depth is filled to the brim with an inviscid fluid We assume that in equilibrium the capillary surface is flat, situated at $z = 1$ and that the capillary surface remains attached to the rim of the container when the surface is disturbed. Given some initial disturbance the free surface will then oscillate about the equilibrium position $z = 1$. Note that in order to study this test problem with our numerical code, all we need to do is prescribe some initial disturbance and take $We = 0$ to that $\partial\phi/\partial z|_{z=0} = 0$ on $\Gamma$.

In order to monitor the energy conservation of our numerical scheme we have to calculate the surface energy $\mathscr{E}_S$, the kinetic energy $\mathscr{E}_K$ and the potential energy $\mathscr{E}_P$ at each time step. For simplicity we neglect body forces so that $\mathscr{E}_P = 0$. The *excess* surface energy is equal to the increase in surface area due to the free-surface displacement,

$$\mathscr{E}_S = |S| - |S_0|,$$

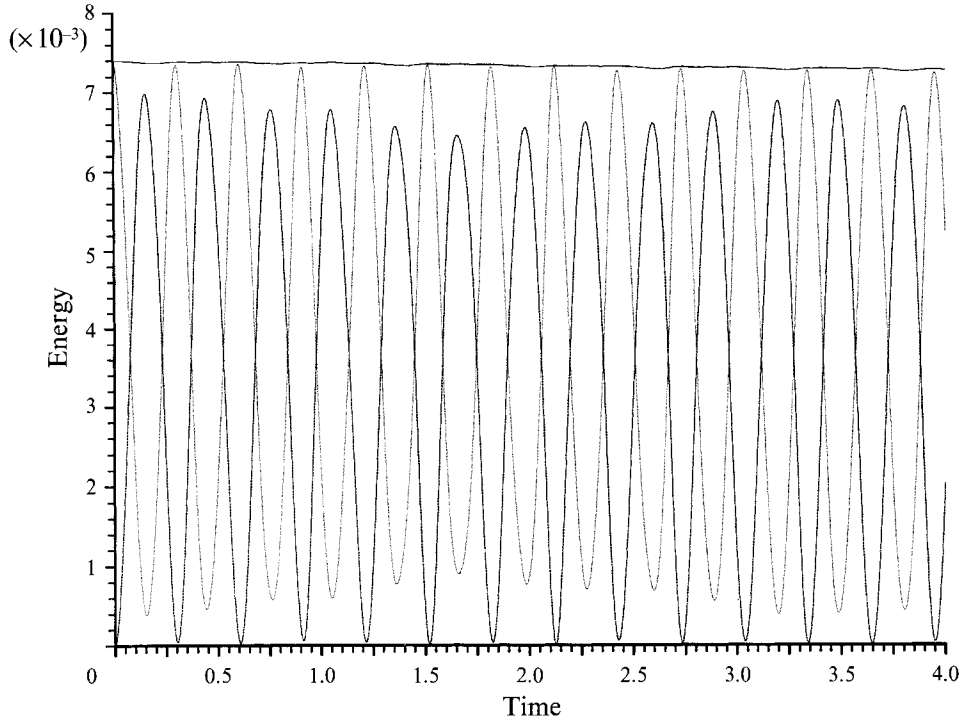


FIGURE 12. Plots of the energies $\mathscr{E}_S/2\pi$ (dotted line), $\mathscr{E}_K/2\pi$ (dashed line) and $\mathscr{E}_T/2\pi$ (solid line) versus time.

with $|S_0| = 2\pi$. The kinetic energy of free-surface oscillations is given by the well-known expression

$$\mathscr{E}_K = \int_S \phi \frac{\partial \phi}{\partial n} r \, \mathrm{d}s.$$

We assume that some initial free-surface elevation is given and that the free surface is at rest at $t = 0$. Energy conservation then implies that $\mathscr{E}_{S,0} = \mathscr{E}_S + \mathscr{E}_K$ where $\mathscr{E}_{S,0}$ denotes the excess surface energy due to the initial disturbance. For the initial disturbance. For the initial elevation of the free surface we take

$$\eta_0(r) = \epsilon(5r^3 - 6r^2 + 1), \tag{A 1}$$

which satisfies the conditions $\eta_0(1) = \eta_0'(0) = 0$ and $\int_0^1 \eta_0(r)\, r \mathrm{d}r = 0$. A straightforward calculation shows that $\mathscr{E}_{S,0}/2\pi = 7.42 \times 10^{-3}$ for $\epsilon = 0.1$ and $\mathscr{E}_{S,0}/2\pi = 2.87 \times 10^{-2}$ for $\epsilon = 0.2$. In figure 12 we have plotted $\mathscr{E}_S$, $\mathscr{E}_K$ and $\mathscr{E}_T = \mathscr{E}_S + \mathscr{E}_K$ as a function of time for the initial disturbance with $\epsilon = 0.1$. The calculation was performed with 40 elements on the free surface, $\Delta t = 1.25 \times 10^{-3}$ and regridding was applied every time step. A calculation in which regridding was not applied at all yielded results that were virtually identical. We observe the oscillatory behaviour of the free surface and kinetic energies; however the total energy does not vary significantly with time and remains more or less constant at its initial value $\mathscr{E}_T = \mathscr{E}_{S,0} = 7.42 \times 10^{-3}$.

In figure 13(*a*) we have plotted $\mathscr{E}_S$, $\mathscr{E}_K$ and $\mathscr{E}_T$ as a function of time for the case $\epsilon = 0.2$ and no regridding. We note relatively large variations in $\mathscr{E}_T$ near $t = 1$ and 1.75. Shortly after $t = 1.75$ the calculation breaks down. In order to explain these results we have plotted the free-surface elevation at $r = 0$ as a function of time in figure 13(*b*). We

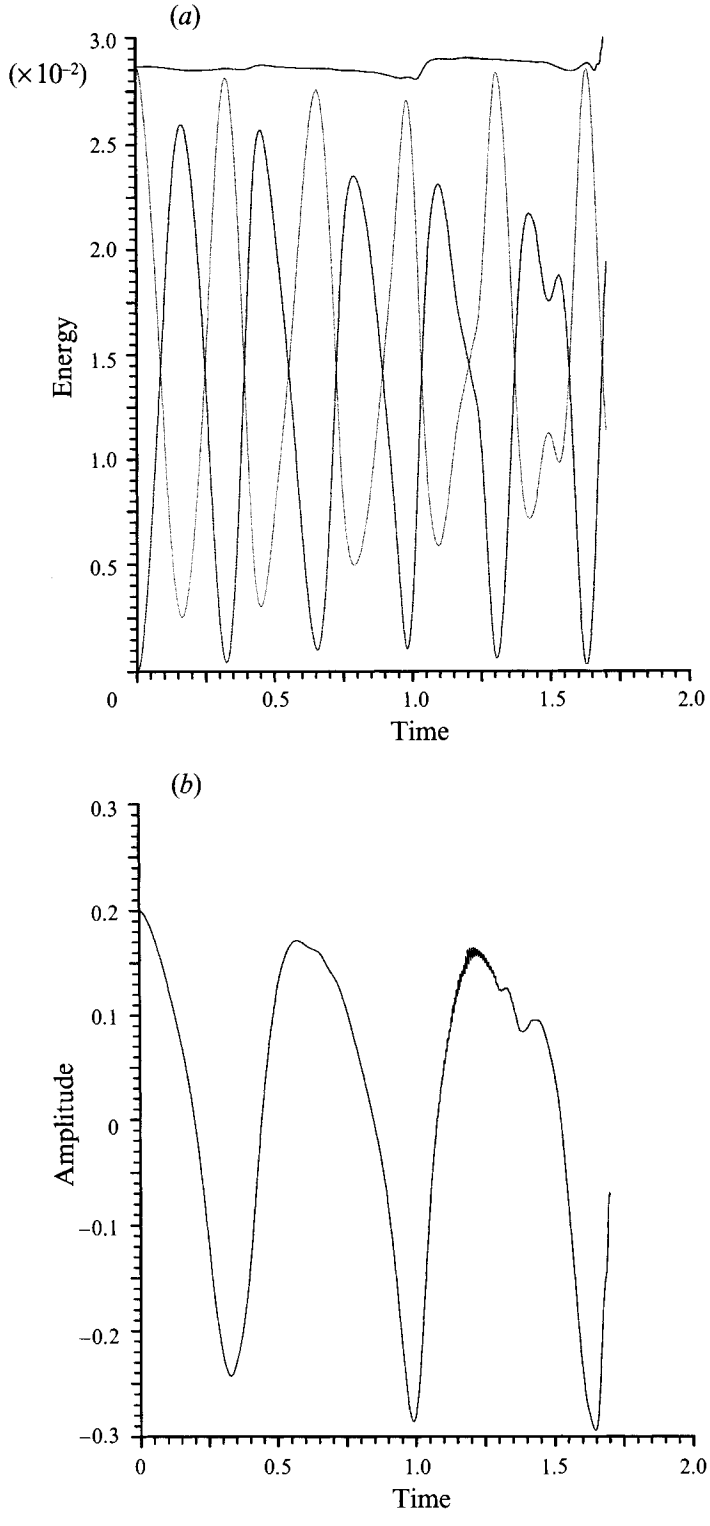


FIGURE 13. (*a*) The energies $\mathscr{E}_S/2\pi$ (dotted line), $\mathscr{E}_K/2\pi$ (dashed line) and $\mathscr{E}_T/2\pi$ (solid line) versus time. (*b*) The amplitude of the free surface at $r = 0$ versus time. No regridding was used in the calculations.

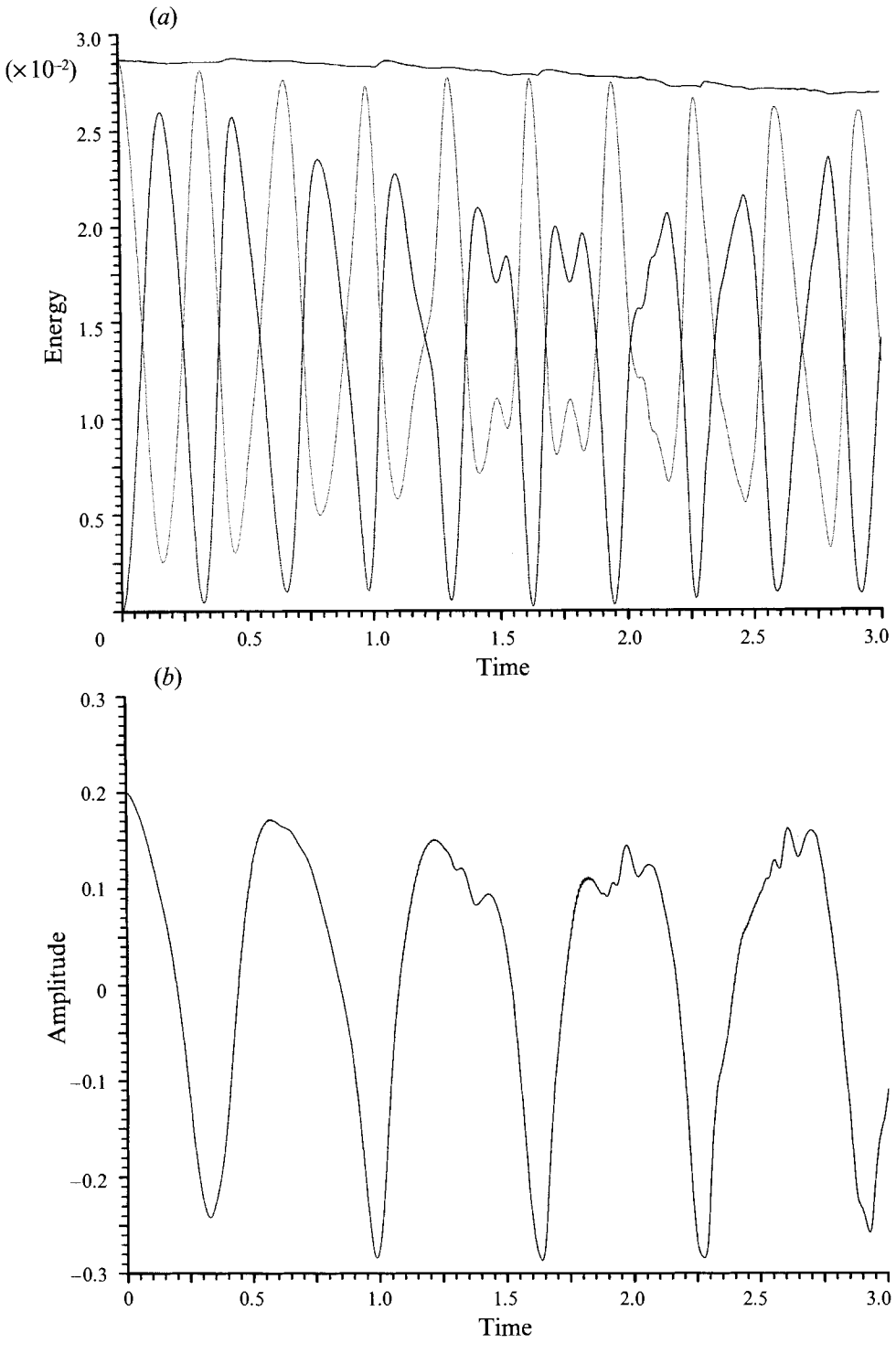


FIGURE 14. As figure 13 but with regridding applied after each time step in the calculations.

note that shortly after $t = 1$ high-frequency oscillations appear which then disappear but subsequently reappear near $t = 1.75$ with increased amplitudes. The increase in the total energy can be attributed to the presence of the high-frequency waves. The breakdown of the calculation is due to the unbounded growth of the amplitudes of the high-frequency waves.

When the calculation with $\epsilon = 0.2$ is performed once more but with regridding applied after each time step, we find that the energy and amplitude vary with time as shown in figure 14$(a, b)$ respectively. We observe that while there is still evidence of high-frequency oscillations, the amplitudes of these oscillations do not grow so as to cause the calculation to break down. The total energy clearly varies with time, decreasing slightly as time increases. It is evident that energy is dissipated as a result of the regridding operation. However, we believe that for the problem under consideration the energy dissipation is not excessive and is unlikely to have a major influence on the results since the time integration is rarely continued for longer than 4 dimensionless time units.

## REFERENCES

ABROMOWITZ, M. & STEGUN, I. A. 1972 *Handbook of Mathematical Functions*. Dover.

DIAS, F. & VANDEN-BROECK, J.-M. 1990 Flows emerging from a nozzle and falling under gravity. *J. Fluid Mech.* **213**, 465–477.

DOLD, J. W. 1992 An efficient integral algorithm applied to unsteady gravity waves. *J. Comput. Phys.* **103**, 90–115.

DOMMERMUTH, D. G. & YUE, D. K. P. 1987 Numerical simulation of nonlinear axisymmetric flows with free surface. *J. Fluid Mech.* **178**, 195–219.

DUSSAN, V., RAMÉ, E. B. & GAROFF, S. 1991 On identifying the appropriate boundary conditions at a moving contact line: an experimental investigation. *J. Fluid Mech.* **230**, 97–116.

LUNDGREN, T. S. & MANSOUR, N. N. 1988 Oscillations of drops in zero gravity with weak viscous effects. *J. Fluid Mech.* **194**, 479–510.

OĞUZ, H. N. & PROSPERETTI, A. 1990*a* Bubble entrainment by the impact of drops on liquid surfaces. *J. Fluid Mech.* **219**, 143–179.

OĞUZ, H. N. & PROSPERETTI, A. 1990*b* Bubble entrapment by axisymmetric capillary waves. In *Engineering Science, Fluid Dynamics, A Symposium to Honor Theodore Yao-Tsu We* (ed. G. T. Yates), pp. 191–202. World Scientific.

PELAKASIS, N. A., TSAMOPOULOS, J. A. & MANOLIS, G. D. 1991 Nonlinear oscillations of liquid shells in zero gravity. *J. Fluid Mech.* **230**, 541–582.

PELEKASIS, N. A., TSAMOPOULOS, J. A. & MANOLIS, G. D. 1992 A hybrid finite-boundary element method for inviscid flows with free surface. *J. Comput. Phys.* **101**, 231–251.

VAN DE VORST, G. A. L., MATTHEIJ, R. M. M. & KUIKEN, H. K. 1992 A boundary element solution for two-dimensional viscous sintering. *J. Comput. Phys.* **100**, 50–63.

VANDEN-BROECK, J. M. 1993 A two-dimensional jet aimed vertically upwards. *J. Austral. Math. Soc.* **34**, 393–400.